ISTANBUL TECHNICAL UNIVERSITY ★ INSTITUTE OF SCIENCE AND TECHNOLOGY

SEMI AUTOMATIC TRUE ORTHOPHOTO PRODUCTION BY USING LIDAR DATA

M.Sc. Thesis by
Arif GÜNAY, Eng.
501051604

Date of submission : 5 May 2007

Date of defence examination: 11 June 2007

Supervisor (Chairman): Prof.Dr. M. Orhan ALTAN
Members of the Examining Committee Prof.Dr. F. Gönül TOZ (İTÜ.)
Prof.Dr. Ferruh YILDIZ (SÜ.)

JUNE 2007

PREFACE

This thesis research has been carried out in Photogrammetry and Geoinformatics Master Course of the Stuttgart University Applied Sciences – Hochschule für Technik Stuttgart (HfT).

I would like to thank all the lecturers of the HfT for giving me a warm welcome and making me always feel as being part of the family. I also would like to thank Professor Michael Hahn for offering me to write this thesis research and Mr. Hossein Arefi for his help and support on this research at the HfT.

My special thanks for Professor M. Orhan Altan from Technical University of Istanbul for giving me an opportunity to do my research at the HfT as my supervisor. And last, but certainly not least, I would like to thank Umut Aydar, Özgür Avşar Esra Erten and Melis Mine Şener for all the support and words of encouragement during my reaserch.

May, 2007 Arif GÜNAY

TABLE OF CONTENTS

TABLE LIST

FIGURE LIST

SEMI AUTOMATIC TRUE ORTHOPHOTO PRODUCTION BY USING LIDAR DATA

SUMMARY

Light Detection and Ranging (LIDAR) has been used for years with a variety of applications, including the efficient creation of digital terrain models (DTMs) for large-scale, high-accuracy mapping. LIDAR technology offers fast, real-time collection of 3-D points so that allows the production of higher-accuracy orthophotos than traditional stereo-compilation methods.

Traditional orthophoto production suffers from the fact that buildings (and any other objects above ground) are not correctly placed in the orthophoto. True orthophoto production overcomes these deficiencies by taking the digital surface model (DSM) into account. However, the resulting true orthophotos still suffer from occluded areas and unsharp edges of buildings and roads. The experimental investigations with different data sets show that it is essential to use high quality DSMs to produce high quality true orthophotos.

In this paper, aspects of the improvement of true orthophoto production will be discussed:
(a) in the first approach which has been widely used in photogrammetry, the DSM is used for generating true orthophotos and (b) in comparison to the DSM based method, semi-automatically collected vector data of buildings are superimposed on DTM and are used as input data for generating true orthophotos in the second method. The processes and problems of both true orthophoto production procedures will be investigated in detail and results include the comparison of true orthophoto productions based on DSM (from first pulse and last pulse measurements) and DTM plus vector data. For the experimental investigation, a LIDAR data set for downtown Stuttgart is used.

LIDAR VERİSİ KULLANARAK YARI OTOMATİK GERÇEK ORTOFOTO ÜRETİMİ

ÖZET

Uzun yıllardan beri orman arazilerinin kontrolü ve yönetimi, su baskınlarına karşı risk analizi gibi çeşitli uygulamalarda kullanılan LIDAR (LIght Detection and Ranging) teknolojisi, son yıllarda temelinde Gerçek Ortofoto üretimine dayalı üç boyutlu şehir modeli oluşturulmasında popüler olarak kullanılmaya başlanmıştır.

Geleneksel Ortofoto üretiminde Sayısal Arazi Modeli'nin (SAM) kullanılması sonucu, binalar ve arazi üzerinde kalan diğer objeler, perspektif iz düşümden kaynaklanan görüntü ötelemesinden dolayı Ortofoto üzerinde doğru olarak konumlandırılamamaktadır. Ortofoto üretiminin, SYM kullanılarak gerçekleştirilmesiyle bu sorunlar büyük ölçüde aşılmakta ve elde edilen Ortofoto "*Gerçek Ortofoto"* olarak adlandırılmaktadır. Buna rağmen, gerçek Ortofoto üretimi farklı sorunları beraberinde getirmektedir. Binaların gerçek konumlarına getirilmesi sonucunda, Ortofoto üzerinde resim bilgisi olmayan alanlar oluşmaktadır. Bunların yanında aşılması gereken diğer bir sorun, gerçek Ortofotoda; yolların, köprülerin ve bina çatı kenarlarının sınırlarının keskin bir şekilde görünmemesidir ve şimdiye kadar yapılan araştırmalarda bu sorunun aşılmasında SYM'nin kalitesinin önemli bir rol oynadığı ve Lazer noktaları ile üretilen SYM'nin tek başına yeterli olmadığı gözlenmiştir.

Bu tez çalışmasında, Ortofotonun geliştirilmesi üzerine uygun methodlar araştırılmış ve iki farklı method test edilmiştir. (1) İlk metod olarak, gerçek Ortofoto üretimi için fotogrametride yaygın bir şekilde kullanılan SYM gerçek Ortofoto üretiminde kullanılmış ve (2) ikinci method olarak, hava fotoğraflarının üç boyutlu değerlendirilmesi ile sayısallaştırılan binaların çatı kenarları, vektör veri olarak SAM'ın üzerine eklenerek gerçek Ortofoto üretilmiştir. Bu bildiride, üretim işlem adımları ve karşılaşılan sorunlara detaylı bir şekilde değinilerek, iki farklı yöntemle

üretilen gerçek Ortofotonun karşılaştırılması anlatılmaktadır. Deneysel araştırma için Stuttgart şehir merkezinin Lidar veri seti kullanılmıştır.

1. INTRODUCTION

1.1. Scope of the Research

The use of LIDAR systems in the areas of Photogrammetry and Remote Sensing is recently increasing in popularity as it allows for direct acquisition of three – dimensional (3D) dense information along homogenous surfaces. Due to its advantages as an active technique for reliable 3D determination, LIDAR has become a rather important information source for generating high quality 3D digital surface models [1]. Up until now, acquisition of 3D information over a surface has been carried out by conventional photogrammetric methods. However, these methods are often rather complicated and the resulting DSM often does not meet the high level of accuracy required for 3D object modelling and true orthophoto production. Recent advances in LIDAR systems make use of efficient DSMs for a variety of studies such as feature extraction, 3D object modelling and true orthophoto generation. Several different approaches have been presented for 3D building extraction and true orthophoto generation based on DSM [2], [3]. However, all methods are principally based on height information and the digital orthoimage is only as accurate as the surface model provided [4]. Even though photogrammetry is still commonly used for GIS data acquisition, in the case of detailed modelling of objects in urban areas it is a very complex, sensitive and time-consuming task [4], [5]. On the other hand, LIDAR provides useful approximations for buildings and other features found in urban areas [1]. As demonstrated in [5], it is advantageous to integrate LIDAR data and digital images for generating a city model. For these reasons, true orthophoto production is becoming an important way to obtain 3D models of a surface, especially for building and city modelling applications.

1.2. Research Goal

In this paper, we deal with automatic and semi automatic true orthophoto production by using LIDAR data and (RGB) digital aerial images for 3D model generation

purposes. Recent experimental investigations have shown that the modelling of DSMs play a vital role in the production of high accuracy true orthophotos. The objective of this research is to improve the quality of true orthophoto, by investigating efficient and accurate DSM creation.

The overall tasks of this research are:

- Terrain and surface extraction from LIDAR data for modeling of a DTM or a DSM
- Digitizing building's outline by using a photogrammetric stereo workstation and blending them with DTM
- True orthophoto generation by using image models and DSM (in two different way; only from LIDAR data or DTM plus vector building outlines)
- Determining suitable approach by evaluating and comparing result of both true orthophoto productions

1.3. Methodology

Two different approaches were investigated for the production of true orthophoto purposes. In the first approach, DSM was modeled only from LIDAR data and taken into account with digital aerial images. The first task was to run rectification process based on reprojection for the true orthophoto production. Rectification process was carried out by two steps. In the first step, pixels from the input images were projected onto the corresponding position on the ground surface (DSM) by using collinearity equation. Then, the matched pixels were reprojected onto the map plane (true orthophoto) from the DSM based on orthogonal projection. In the second step, grey levels from the input pixels were interpolated and assigned to the output pixels by using bilinear resampling method. During the rectification process, the visibility map was checked to locate occluded areas. As a result of rectification processes, all buildings were repositioned correctly and occluded areas were marked by a specified colour in the overlapped orthophotos. The second task was to run mosaic process to fill all occluded areas and merge the overlapped orthophotos as a form of mosaic so-called "*True Orthophoto"*. In the first step, all parts of the occluded areas were filled with corresponding image information which was visible in one of the adjacent orthophotos based on the results of the visibility test. In the second step, all

overlapped orthophotos were merged as a form of mosaic where the seamlines defined.

In the semi automatic approach, for modeling of the DSM not only utilized from LIDAR data but also digitized roof borders and ridges were used. Firstly, terrain texture was extracted from the LIDAR data instead of the surface texture so that 3D points of buildings and trees were removed. Then, roof borders and ridges were digitized by photogrammetric stereo workstation and superimposed on the DTM for the purpose of DSM creation. Hence, DTM plus semi-automatically collected vector data were taken into account with the digital aerial images in order to generate true orthophoto in the second approach. The last task of true orthophoto production was to merge all overlapped orthophotos and fill in occluded areas with real image information. Accordingly, mosaic process was run as it was done in first approach so that all orthophotos were merged and occluded areas were filled. The main steps for the automatic and semi automatic true orthophoto production are summarized by the workflow as shown in fig. 1.1.

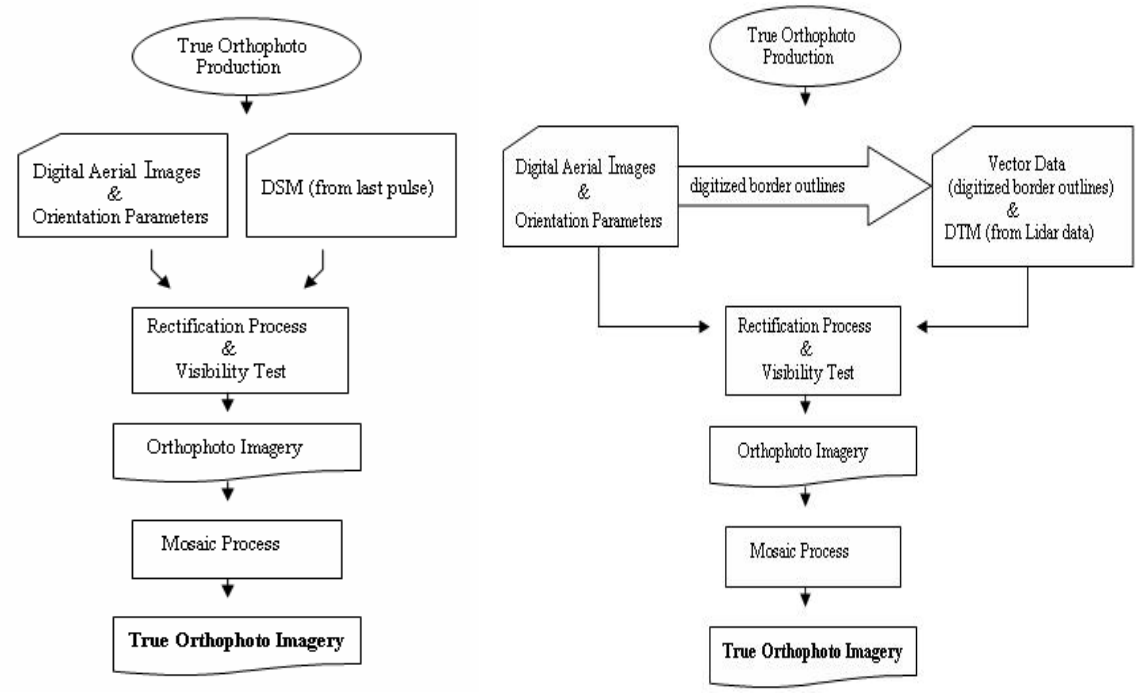

Figure 1.1: (left) Workflow for the automatic true orthophoto production and (right) Workflow for the semi automatic true orthophoto production

1.4 Data and Software used

For the experimental investigation a LIDAR test data and RGB digital images covers the downtown area of Stuttgart (in Germany). The test data sets have been provided by TopScan Company, in Germany [6]. LIDAR test data has been recorded as the first pulse and the last pulse by ALTM 2050 Laser scanner with a density of 4.8 per m². RGB digital images have been taken simultaneously by using the Rollei AIC-modular-LS digital metric camera with a 20cm ground resolution.

Table 1.1: Airborne Laser Scanner data

No	Specification	Data
1	Capture Period	April 2006
2	Flight altitude	1100 meter
3	Pulse frequency	50000 Hz
4	Wavelength of the Laser	1064 nm
5	Measurement density	~ 4.8 per m^2
6	Swath width	~ 600 meter
7	Instrument	ALTM 2050 laser scanner

Table 1.2: Digital Images data

No	Specification	Data
1	Capture Period	April 2006
2	Flight altitude	1100 meter
3	Sensor size	X=48.96mm, Y=36.72mm
4	Scanning Resolution	5440 in X and 4080 in Y
5	Pixel size	9 micron in X and Y
6	Ground Resolution	~ 20 cm
7	Instrument	Rollei AIC-modular-LS
8	Color Type	RGB
9	Format	Tif

As for the software, OrthoBox photogrammetric software package which consists of OrthoMaster for orthophoto generation and OrthoVista for orthophoto mosaicking and radiometric image enhancement were used. Additionally, DTMaster – digital photogrammetric system was used for efficient quality control of DTM and LIDAR data [7].

1.5. Thesis Contents

This paper is organized as follows: in the following two Chapters, LIDAR systems, orthophoto and true orthophoto imagery are shortly explained. Chapter 4 describes a proposed algorithm for the investigation. Comparisons of the achieved results are mentioned in Chapter 5.

2. LIDAR

2.1. Introduction

LIDAR, also referred to as Airborne Laser Scanning (ALS), is much the same as RADAR, with the exception that lasers, not radio waves are used. Also, the output product of LIDAR is very different in nature from RADAR. Rather than an image, the raw output is a file of x, y and z coordinates. LIDAR technology has existed since the 1980's, but has only recently become a commercially feasible geomatics product.

There are three basic types/forms of LIDAR:

1. **DIAL** (Differential Absorption LIDAR): This LIDAR is used to study aerosols in the atmosphere. It is generally ground based and is shot upwards into the atmosphere.

2. **Doppler LIDAR**: This LIDAR is used to measure the velocity of moving targets.

3. **LIDAR altimetry**: This LIDAR is used to measure the distance between the source of the LIDAR and a distant point. It is generally gathered from an airborne platform and is used to map the topography of the ground.

This report deals with LIDAR altimetry. This type of LIDAR collection system uses a powerful laser sensor comprised of a transmitter and receiver, a geodetic-quality Global Positioning System (GPS) receiver and an Inertial Navigation System (INS) unit or the inertial measurement unit (IMU), as it is often called [8]. The laser sensor is precision mounted to the underside of an aircraft. Once airborne, the sensor emits rapid pulses of infrared laser light, which are used to determine ranges to points on the terrain below. Laser scanner for topographical applications generally operate with a wavelength of about 0,8 µm to 1,5 µm, i.e. in the near infrared region so that in principle operations during nights are possible [9]. Most LIDAR systems use a scanning mirror to generate a swath of light pulses. Swath width depends on the mirror's angle of oscillation, and ground-point density depends on factors such as aircraft speed and mirror oscillation rate. Ranges are determined by computing the amount of time it takes light to leave an airplane, travel to the ground and return to

the sensor. A sensing unit's precise position and attitude, instantaneous mirror angle and the collected ranges are used to calculate 3-D positions of terrain points. As many as 10,000 positions or "mass points" can be captured every second. Although features such as buildings and automobiles are included in the accompanying figures, these can be removed from DSMs through post-processing filtering techniques. Hence, the ground can be modeled as a "bare Earth" DTM [10].

A generalized aerial LIDAR acquisition and processing workflow consists of the following three steps: 1) Data acquisition 2) point cloud classification and surface estimation, 3) 3D visualization.

Typically the data acquisition - point cloud generation (and sometimes the point cloud classification), is handled by the data provider and is not a significant concern to the researcher seeking LIDAR products for science applications.

2.2. Data Acquisition

Acquisition of aerial LIDAR data utilizes a pulsed laser ranging system operating at 10s of thousands of pulses per second mounted in an aircraft equipped with a kinematic Global Positioning System (GPS) to provide precise positioning information for the aircraft. An accurate inertial measurement unit (IMU) monitors the orientation (roll, yaw and pitch) of the aircraft. By scanning the laser pulses across the terrain using a rotating mirror, it is possible to quickly and economically acquire hundreds of millions to billions of individual point measurements of the absolute x, y and z coordinates of the ground surface and vegetative cover in a survey area (fig. 2.1.a). LIDAR instruments typically sample the ground surface multiple times per square meter and provide an absolute vertical accuracy of 5-10 cm. These LIDAR measurements are commonly referred to as the 'point cloud' (x, y, z plus attributes) and typically consist of 100s of millions or billions of returns depending upon the size of the survey area and resolution of the data being acquired (fig. 2.2) [11]. Early versions of laser altimeters measured the distance to the first feature reflecting the laser pulse. In areas of dense vegetation that is usually the top of the vegetation canopy (fig. 2.1.b) [12]. The most important feature of recent airborne LIDAR systems is its ability to discriminate first and last pulse reflections. A laser pulse that is fired over vegetation usually has multiple reflections. Some particles of the laser pulse may be reflected by leaves or branches of trees often

represented in the first returning pulse (fig. 2.3.a). Others may be reflected by the ground and the last returning pulse is most likely to be reflected by the terrain surface beneath trees (fig. 2.3.b) [13]. This ability to segregate the point cloud data based upon the origin of the return significantly enhances the utility of these datasets to a wide variety of user communities.

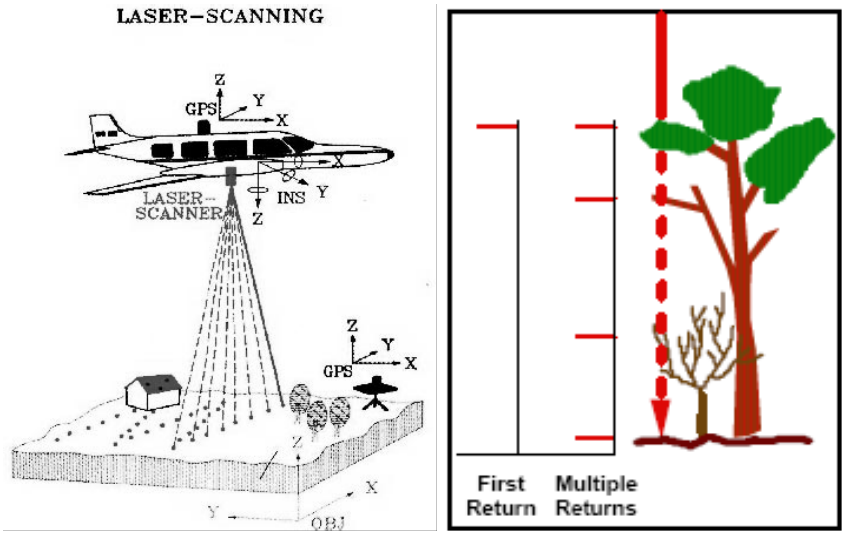

Figure 2.1: (a) (right) Laser scanning principle and (b) (left) first pulse reflection from vegetation areas [12]

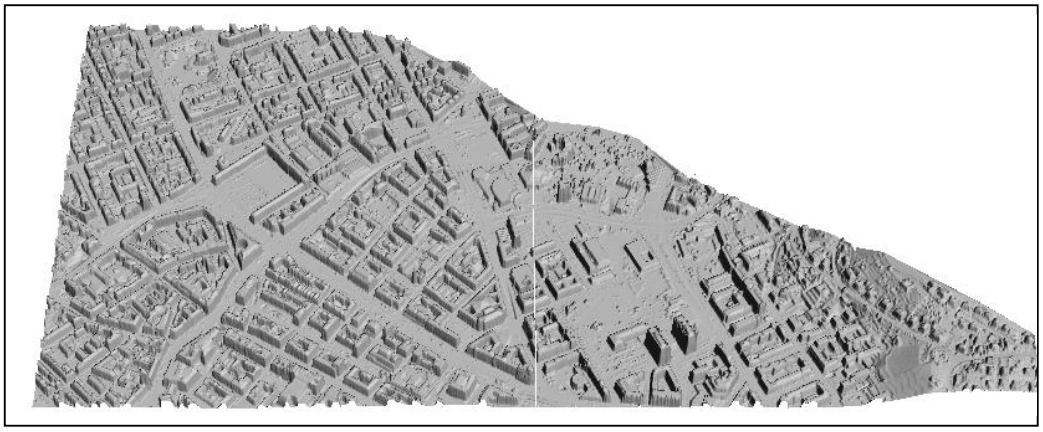

Figure 2.2: Shaded relief made from a point cloud

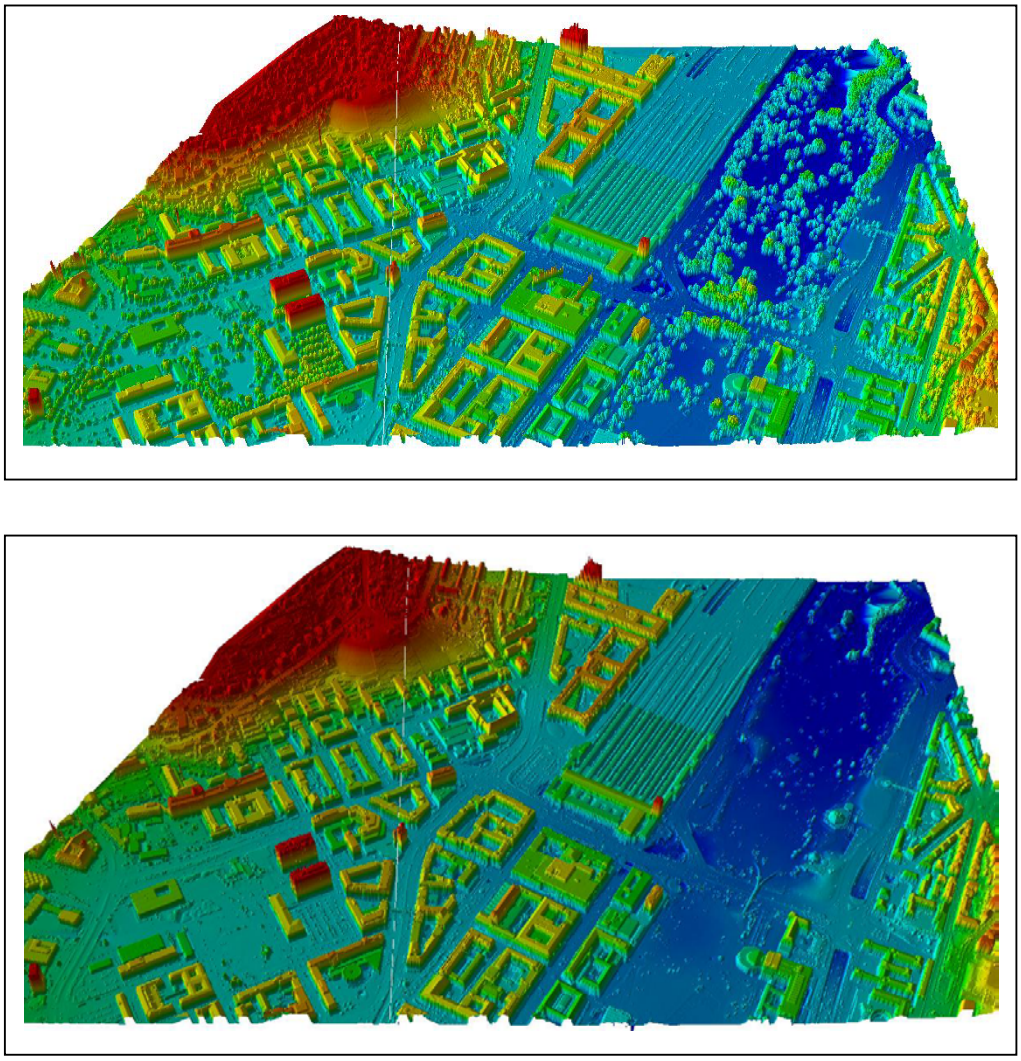

Figure 2.3: (a) (Above) First pulse measurement and (b) (Below) Last pulse measurement

2.2.1 Point measurement

3- Dimensional co-ordinates of a point is determined in a desired reference system by combining the laser ranging system, GPS, and IMU on an aircraft as mentioned above.

As shown fig. 2.4, using vector notation the computation of **vector p** is obtained through the addition of

⇒ the **measurement vector d** between sensor and object point

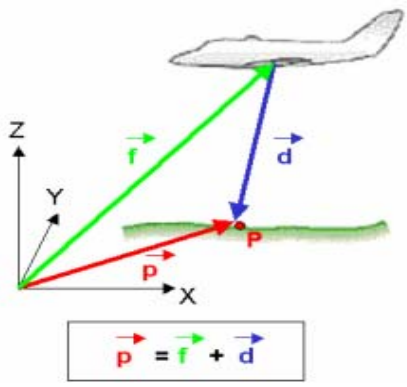

Figure 2.4: Vector notation for computing a 3D point

⇒ Lasers can precisely measure distance **vector d** from a sensor to the ground using speed-of-light calculations.

The **absolute value (or norm) |d| of the measurement vector** is computed by half of the distance that the laser beam travels between the emitter and the object point (and reverse) (see also fig. 2.5). This distance results according to the path-time-law using the speed of light and the very precise measurement of the travel time Δt into.

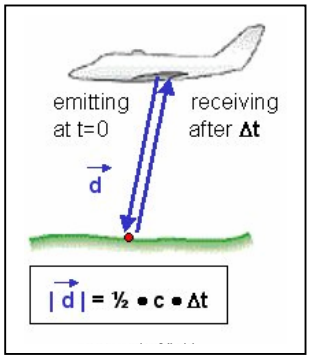

Figure 2.5: Computation of the range

⇒ the **postion vector f** towards the sensor is determined through combined (GPS-/IMU-measurements) [9]

Using only one GPS receiver onboard the moving platform, its position cannot be determined with sufficient precision. Two or more GPS receivers, logging data at the same rate, are deployed at known ground locations during each flying mission. In airborne GPS techniques that support photogrammetric mapping, kinematic GPS post-processing techniques yield aircraft/sensor trajectory as a series of 3-D positions. GPS data from the aircraft and multiple ground stations are processed

together using sophisticated kinematic GPS post-processing software. The use of two or more ground stations provides quality control and improves the accuracy of the kinematic trajectory. As a result, the position (x, y and z) of an airborne GPS antenna at an interval of 0.5 or one second is calculated. During a flight mission, an aircraft rotates on three different axes, commonly known as roll, pitch and yaw (analogous to w, j and k in photogrammetry) which are monitored by an accurate inertial measurement unit (IMU). These axes determine an aircraft's *attitude*, and this orientation affects the antenna's spatial relationship relative to sensor origin as an aircraft moves through the air. Subsequent to GPS processing, raw INS data and GPS trajectory are combined using advanced Kalman Filtering techniques. The outcome is a complete set of exterior orientation (EO) data (x, y, z, w, j, k) for sensor origin and output at a rate of 50Hz [10]. Mass points (first and last return positions) then are computed using a combination of measured ranges, mirror scan angles and EO data. Various calibration parameters are input at this stage. Calibration data derived from control points in overlapping flight strips and from the acquisition of data over reference surfaces. The latter should be ideally areas with very less surface texture and with a nearly constant elevation (e.g. sport fields). For the stabilization of the co-ordinate computation the results of independent terrestrial (GPS- or tachymetry-) measurements are also introduced [9]. In addition, the parameters of flying height, swath angle, scanner rate, flight-strip side lap and aircraft velocity determine the point density as a system moves through the air, and these parameters are tailored to accommodate project requirements. An aircraft flies a regular pattern over a project area, for example, and a focused eye-safe infrared laser sends a variable number of pulses (10 KHz is common) to the ground in a fan array across the flight path [10].

2.2.2 Point characteristic

Objects on the ground differ in material composition and height, the signal strength of the reflected pulse (i.e., the echo of the emitted pulse) is also recorded. Several reflections of a pulse maybe detected. The first reflected pulse is assumed to contain more hits off vegetation than the second pulse. Therefore, first pulse returns are used in orthophoto production and forestry and vegetation inventory applications, while second pulse returns are used for bare earth measurement applications. Just as the return waveform is used to measure the return time of a pulse, most systems also use it to measure the strength of the returned pulse. The materials on the landscape have

different spectral characteristics and because of this, a low resolution image of the landscape can be obtained from the strength of the returned pulse. Typically, the radiation used in LIDAR is in the IR part of the EM spectrum. Therefore, materials like vegetation will tend to appear bright, earth and asphalt will appear dark, and deep-water bodies will absorb radiation (see fig. 2.6 also). Because of this reflectance can be used to some extent for classification. Some LIDAR systems also capture imagery during scanning. Therefore, an RGB triplet can also be associated with each point [14].

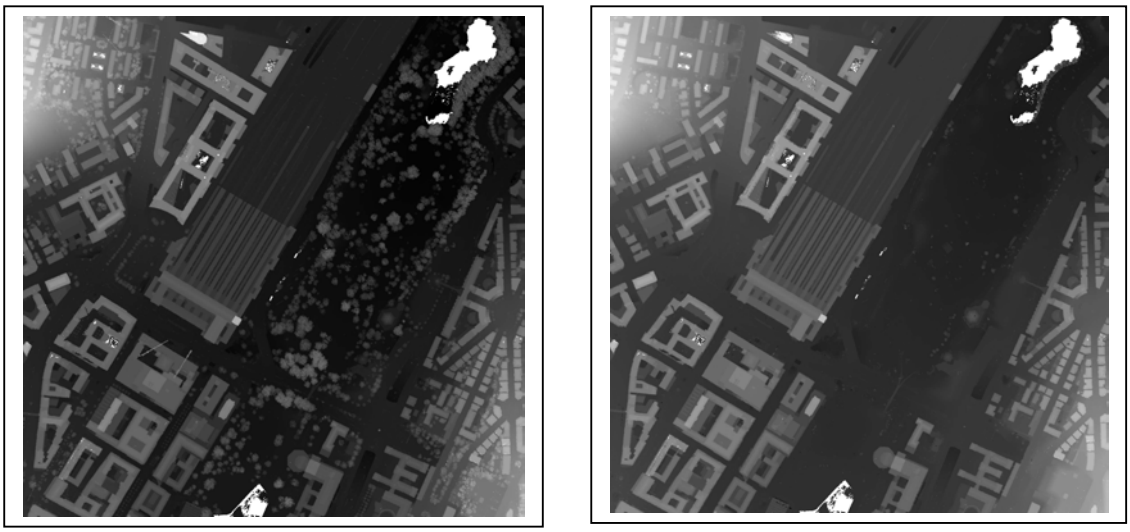

Figure 2.6: (left) (a) First pulse intensity image and (right) (b) last pulse intensity image

2.3. Point Cloud Classification and Surface Estimation

The large volume of data points generated by a LIDAR system poses a significant challenge in terms of data management and raw processing power. For example, several hundred million points typically are captured for a medium-sized county. Many applications, for example, contouring, require a bald-earth DTM. Unfortunately, the raw data points captured by LIDAR do not constitute a bald-earth DTM. Even though most LIDAR systems can measure "last-return" data points, these "last-return" points often measure ground clutter like shrubbery, cars, buildings, and even the canopy of dense foliage. Consequently, raw LIDAR points must be post-processed to remove these undesirable returns [15]. Because most modern LIDAR instruments are capable of recording multiple returns from each outgoing laser pulse, it is possible to classify the individual laser returns by applying

a filtering algorithm to differentiate ground returns from vegetation returns [11]. LIDAR points may represent ground clutter like trees, cars and buildings. Many users require a "bare-Earth" elevation model, but others require a canopy surface that includes trees and buildings. Consequently, it's important to intelligently reduce the size of LIDAR datasets to manageable levels and filter out unwanted information—a process sometimes referred to as classification. A number of algorithms have been developed for semi automatically/automatically extracting the bare earth from point clouds obtained by ALS and InSAR. While the mechanics of some of these algorithms have been published, those of others are not known because of proprietary restrictions. Some comparison of known filtering algorithms;

- ⇒ (Lindenberger, 1993) adopts the filtering approach and uses a morphological filter to eliminate non-ground points. He applies an opening to the LIDAR data using a horizontal structural element. This is followed by an autoregressive process to improve the results. (Kilian et al, 1996) also use a morphological filter. They then perform a weighted smoothing of the surface based on the distance of the individual LIDAR points to the opened surface. They conclude that the size of the structural element used for the opening is a critical parameter for which there is no single optimal value. They suggest the usage of multiple openings with different sizes of structural elements.

- ⇒ (Vosselman, 2000) presents an approach for LIDAR data filtering that is closely related to a morphological filter. He estimates an optimal filter function by analyzing the height differences between ground points in training data sets. He shows that his slope-based filtering is superior to a morphological filter with a horizontal structural element.

- ⇒ (Kraus, Pfeifer, 1998) describe an approach for DTM estimation based on a robust, finite-element estimation for data with an asymmetrical error distribution. Our approach is an extension of this work and is described in more detail later.

Additionally, there are several commercial packages available for the post processing of LIDAR measurements. The (Optech, 2001) LIDAR system comes with a post-processing package. The algorithm used for the filtering is not published. The parameter set for the algorithm and the artifacts observed in the processed data

suggest that the algorithm is based on a morphological filter. (TerraSolid, 2001) offers a variety of LIDAR processing modules,

Including TerraScan for the filtering and thinning of LIDAR data. This package includes different methods for slope-based filtering and thinning of LIDAR data. (INPHO GmbH, 2001) offers a product called SCOP for the derivation of DTM's and contours from various sources, including LIDAR data [15]. In this research, DTM was extracted by using morphological filter. J. Lindenberger approach regarding the morphological filter is reviewed below.

For the purpose of discussion a point cloud, V, will be treated as a set of attributed points in three-dimensional space as demonstrated in figure 2.7.a. Where, v, is an attributed point with coordinate triplet x and attribute a; V = {v|v(x 2 R3, a 2 R)} [14].

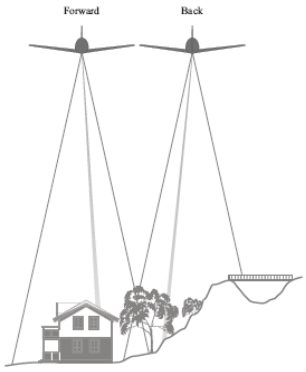

Figure 2.7: (a) Airborne laser scanning. The landscape is scanned in strips, and the scans from the strips are combined to form a point cloud.

The attribute of a point can take on two values, 0 or 1, denoting object and bare earth respectively. Filtering is the removal from V of points with label 0. The removal of zero labeled points yields the set of bare earth points B. Therefore, before filtering can be done the ALS points have to be attributed or labeled.

2.3.1 Review of the J. Lindenberger approach

⇒ Morphological filter - J. Lindenberger: 1993

Assumption - The lowest points in a neighborhood belong to the bare earth.

This filter is based on the concepts of mathematical morphology, which is a settheoretic method of image analysis providing a quantitative description of geometrical structures. The algorithm is applied to ALS scans. In this algorithm (Lindenberger, 1993; Petzold et al., 1999), first a rough terrain model is calculated by the lowest points found in a moving window of rather large size. All the points with height difference exceeding a given threshold are filtered out, and a more precise DTM is determined. Figure 2.7.b shows an example of how the algorithm works. This step is repeated several times, reducing the window size every time. The result is influenced by the final window size and the final threshold below which points are expected to be terrain points. A small window size leads to points on large buildings remaining in the file of the so-called ground points. A large window size smoothes the terrain and removes discontinuities. A high threshold value that is accepted in the final step leads to many vegetation points classified as ground points, and a small threshold again removes small terrain discontinuities. The parameters depend on the morphology of the terrain and have to be different for flat, hilly and mountainous regions [14].

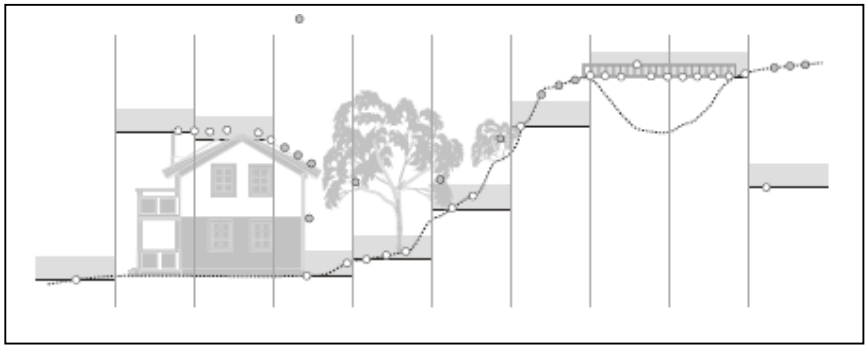

Figure 2.7: (b) Morphological algorithm. White circles are classified as bare earth and gray circles as object [16].

2.4. 3D Visualization

Airborne laser scanning delivers a point cloud. These points in 3D can be used to visualize the data and with that, visualize the area that is surveyed. This 3D visualization can be used for a large amount of reasons such as 3D feature extraction and modeling.

Once the data is collected and processed, it is possible to create any visualization within a short time, depending on the size of the dataset. There are basically three forms in which 3D data exists:

⇒ **Point cloud**

A point cloud is a (large) collection of points consisting of an x-, y- and z-coordinate.

Figure 2.8.a shows a point cloud. It is easy to see that this is not an ideal representation of the outside world. This is because there is not a surface, just a large number of individual points.

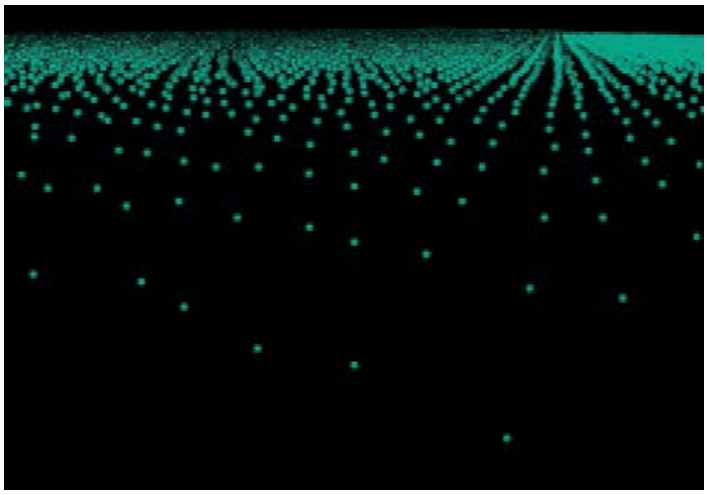

Figure 2.8: (a) 3D Point cloud

⇒ **Grid**

Grids can be constructed from point clouds. First you choose a grid cell size and then the heights from the point cloud will be interpolated into this grid. Grids can be used in many applications. In this research the main tool was MicroStation with the extension tools TerraScan and TerraModeler. The interpolation methods consisted of respectively the Inverse Distance Weighted method and Kriging. In fig. 2.8.b you can see a picture that is made by connecting the surface heights from a grid.

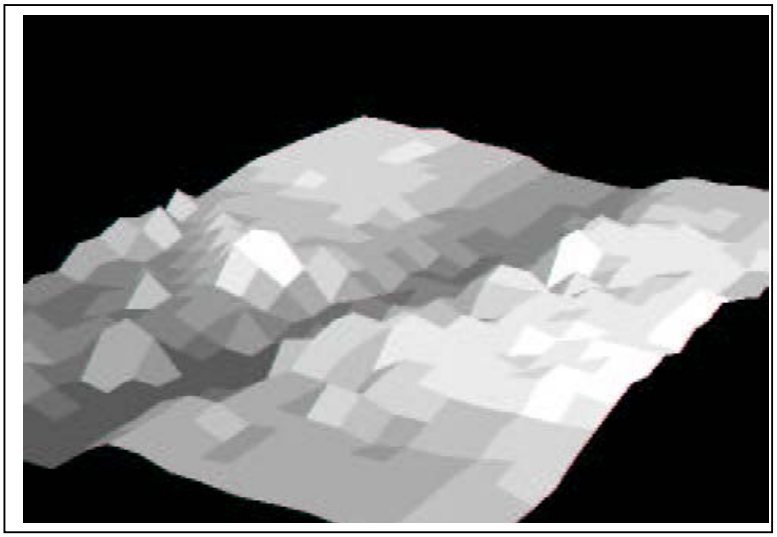

Figure 2.8: (b) A visualisation made from a grid.

⇒ **Triangular Irregular Network (TIN)**

As the name indicates, a TIN is a network set up by irregular triangles. With the point cloud as a basis, forming triangles within the original point data forms the TIN. This gives better detail than a grid, but is also computational more expensive. Fig. 2.8.c shows a TIN.

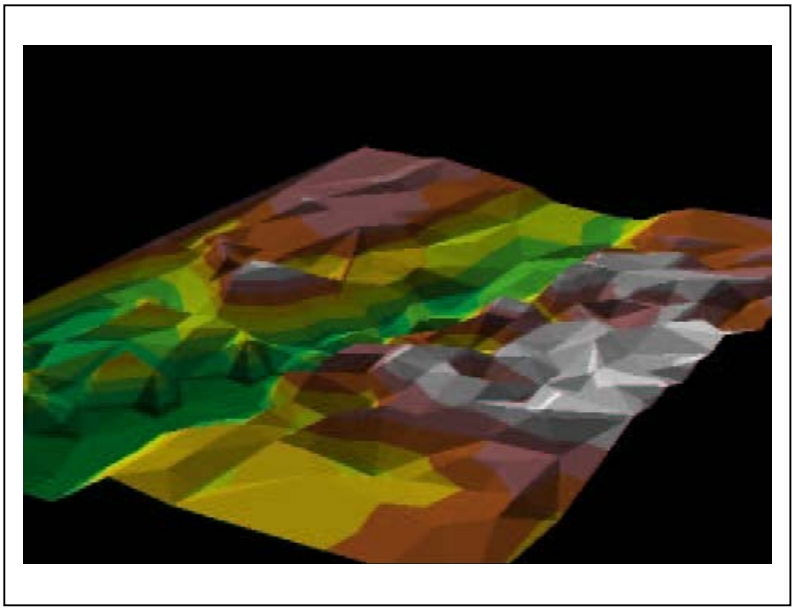

Figure 2.8: (c) A colour-coded TIN.

⇒ **Drapes:**

Drapes are an often-used form of 3D visualisation. The idea is to let an image (in our case true orthophoto) follow the surface of the laserdata. You can use either a grid or a TIN and drape a true orthophoto on top of the surface (see fig. 2.8.d).

Figure 2.8: (d) A true orthophoto draped over a DSM.

Using a grid or a TIN gives slightly different results. A grid usually works faster but has fewer details. A TIN is a lot slower, but provides better results, especially on vegetation and rooftops [16].

3. ORTHOPHOTO IMAGERY

3.1. Introduction

Any aerial photographs exhibit a characteristic known as *relief displacement*. Relief displacement is the geometric distortion that occurs due to elevation differences in the terrain being photographed. Objects of higher elevation, like buildings, hills, and trees, will be displaced radially outward from the center of the photograph. The greater the elevation of the object, and the further it is from the center-of-view, the greater the radial distortion. The process of ortho-rectification corrects these distortions by performing, on the image, a mathematical transformation that takes into account the shape of the terrain in the form of a digital terrain model (DTM). In traditional digital orthophotography, objects like buildings and bridges are not modeled in the DTM. Therefore, these features are distorted from their true location in the final orthophotography. This distortion shows up in the form of leaning buildings and warped bridges. In severe cases, this distortion can be aesthetically displeasing and may impact the usefulness of the orthophotography. For example, a tall building may "lean" over a street, hiding information like manholes, fire hydrants, and utility poles. Complex, multi-level freeway interchanges appear badly deformed. When a vector GIS layer is overlaid with the imagery, building outlines do not match up with the imagery representing the tops of the buildings, and vector road edges will appear as passing through buildings.

As for true orthophoto, it overcomes such deficiencies by taking the DSM into account instead of DTM during the rectification process. In a "true orthophoto," we move objects like buildings and bridges back into their true location (hence the term "true orthophotography"), and replace the "blind spots" that are left behind with real imagery (see also fig. 3.1) [17]. A discussion of our approaches for creating "true orthophotography" describe in the chapter 4.

Figure 3.1: (left) orthophoto and (right) true orthophoto

3.2. Relief Displacement

The lower the flight altitude is, the higher are the relief displacement. In the nadir point there are no relief displacements, but these increase with the distance to nadir. If h is the height of an object on the ground (i.e. a building), H is the flight altitude above the base of the object, and *rt* is the distance to the image center, the relief displacements in the image is calculated by following equation:

$$\Delta r = \frac{h \cdot r_t}{H}$$

Fig. 3.2.a illustrates that a high flying altitude results in smaller relief displacements.

A real world example is illustrated on fig. 3.2.b.

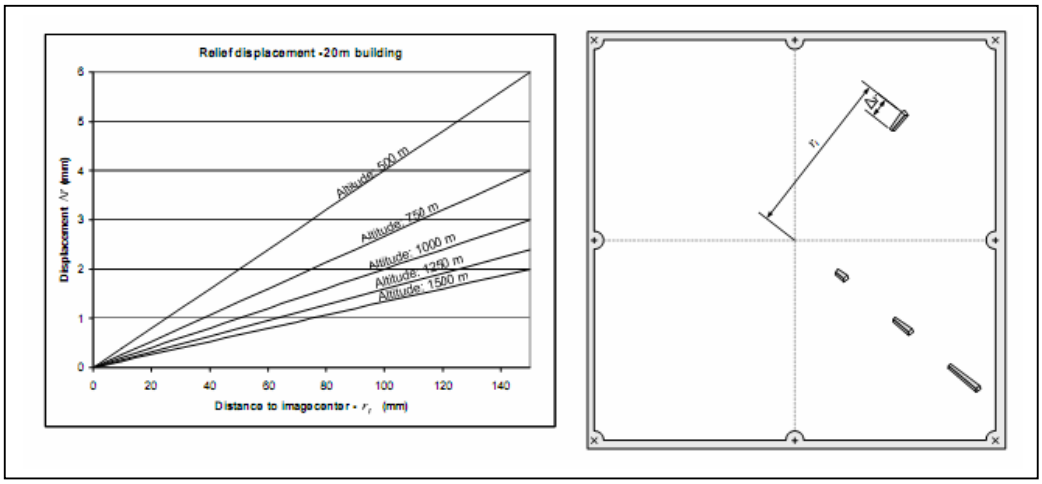

Figure 3.2: (a) Relief displacement increase towards the edge of the image or when the flight altitude is decreasing. The displacements are always oriented away from the nadir point [18].

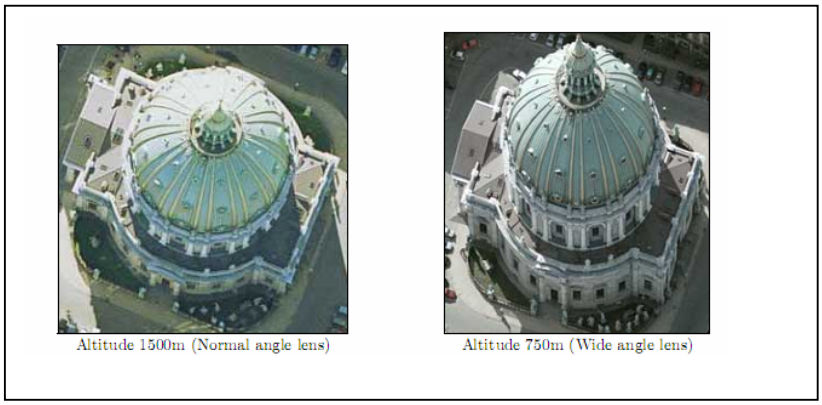

Figure 3.2: (b) The two images above are taken from approximately the same position, but at different altitudes. The relief displacements are significant smaller when the flight altitude is higher. The church on the image is approximately 70 meters tall [18].

3.3. Orthophoto Generation

Existing imagery may be resampled to produce a new image that conforms to specific geometric properties, such as the production of a vertical view from oblique imagery. This may be a one-to-one process, where a single source image is modified into another resampled one, as is commonly the case when producing an orthophoto,

or a many-to-one process, whereby a new image contains parts from multiple images as is the case in mosaicking. Resampling is typically a two step process comprising:

⇒ The establishment of a geometric correspondence between the coordinate systems of the source image s(x, y) and the resampled image r(x′, y′), and

⇒ The establishment of a function to express the radiometric relationship between the two images

Orthorectification is a special case of image resampling whereby the effects of image perspective and relief displacement are removed so that the resulting orthoimage has uniformly scaled pixels, resembling a planimetric map. The two basic approaches to orthoimage generation are forward and backward projection (see also fig. 3.3). In forward projection, pixels from the source image are projected onto the DTM to ascertain their object space coordinates, which are subsequently projected into the orthoimage. In backward projection, the object space coordinates are projected into the source image to derive the radiometric information for the corresponding orthoimage pixel. In either case, image resampling is required to account for terrain variation and perspective effects. Orthophoto generation typically proceeds following a differential rectification, using the collinearity equations to describe the above mentioned geometric relationship between the two coordinate systems. In analog and analytical applications orthoimage generation was a time-consuming process that often required the use of dedicated hardware. With the use of digital imagery, orthorectification was one of the first photogrammetric processes to be automated, and orthoimagery gained renewed popularity in the geospatial user community [19].

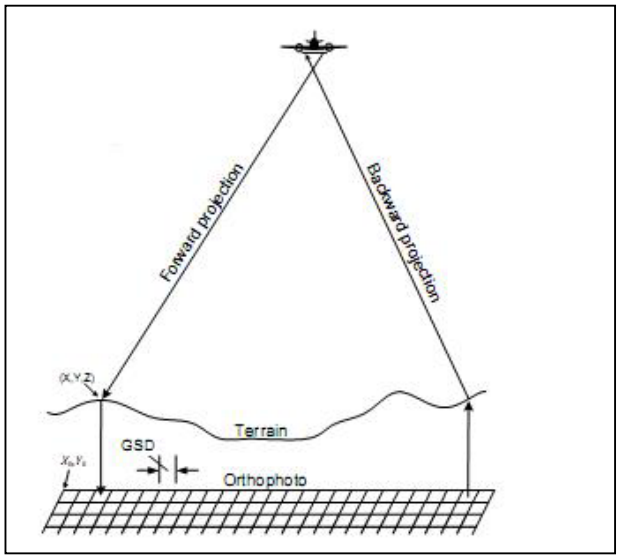

Figure 3.3: The basic idea of forward and backward projection [18]

Digital photogrammetric Workstation (DPW) software input requirements for orthoimage generation include triangulation results and a DTM. The main factors affecting the accuracy of the resulting orthoimage are the spatial resolution of the source image, the accuracy of triangulation, and the accuracy and resolution of the DTM. Beyond these factors, a common problem with orthoimage generation is building lean, the effect of building displacement in urban scenes. The problem and its treatment are demonstrated in figure 3.4. The figure illustrates the progressive correction of orthophoto distortions and displacements according to the availability of certain input sources. Without a detailed DTM it is impossible to correct terrain variations, as demonstrated by the distorted orthophoto grid in figure 3.4.c. Today, most orthoimage generation modules support at least the use of a DTM to correct for these distortions as demonstrated in figure 3.4.d. By using as additional input feature files that model buildings or structures with significant height, the position of these features can be corrected as demonstrated by figure 3.4.e. The building roof is repositioned to reflect its true position in an orthographic projection. However, this repositioning has the effect of leaving a shadow of the building, the orthophoto, corresponding to the area covered by the oblique building image. This effect is commonly referred to as building lean. This effect can be corrected by using available supplemental images that reveal areas hidden in building shadow (fig. 3.4.f) [19].

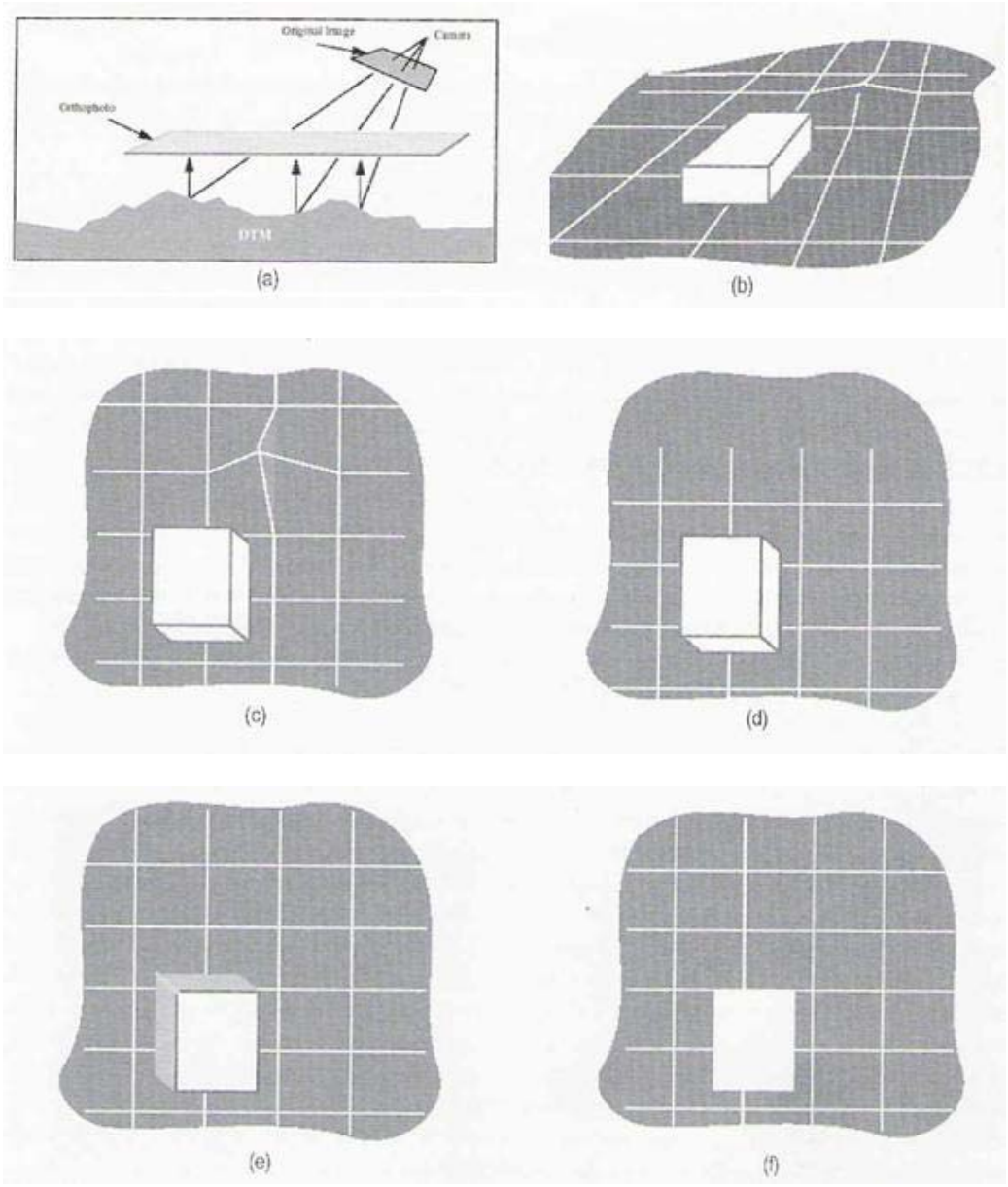

Figure 3.4: Approaches to removing the effects of building lean from an orthoimage. (a) Orthoimage generation geometry, (b) raw image, (c) Orthorectification from triangulation, but without a DEM, (d) Orthorectification from triangulation and a DTM, (e) Orthorectification from a DTM and feature information, but no supplemental imagery, (f) same inputs as previous, but with supplemental imagery to fill in shadows [19].

3.3.1 Mosaic process

Joining two or more contiguous orthoimages to create large coverage image maps is accomplished through image mosaicking (fig. 3.5). The general requirement to

produce a mosaic is contiguous orthorectified images (although it is possible to create a mosaic from raw imagery). The process involves resampling all input images into a common spatial resolution. The user typically has complete control over the positioning of seam lines. Automatic (or manual) histogram matching techniques are employed to smooth out radiometric differences among the input images and to optimize the dynamic range of the mosaic.

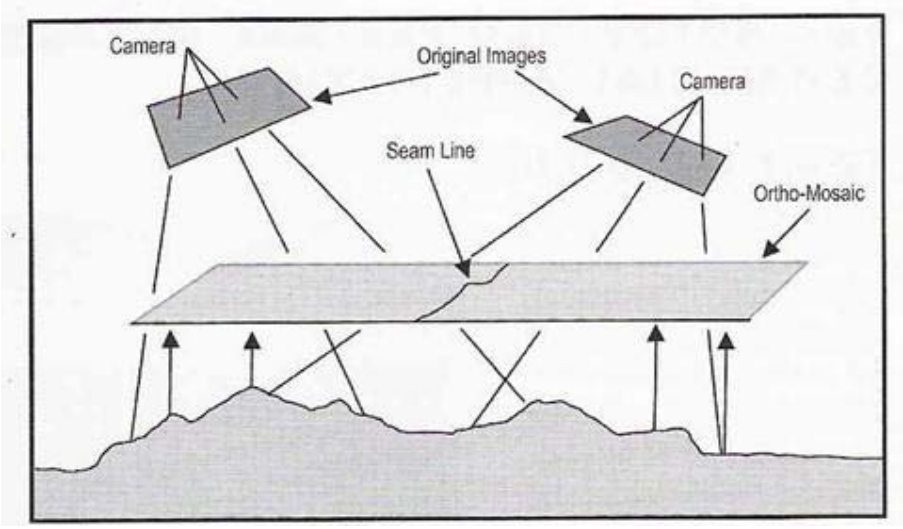

Figure 3.5: Image mosaic geometry [19].

Histogram matching techniques, e.g., image dodging, are used to smooth radiometric unevenness among different images that compose a mosaic. In histogram matching, a lookup table is generated to convert the histogram of one image to resemble or match the histogram of another. The matching process is based on the assumption that differences in global scene brightness are due to external factors such as atmospheric conditions and sun illumination. Therefore, all pixels in a particular match are radiometrically adjusted in a similar manner. Fig. 3.6 demonstrates histogram matching applied to a mosaic created from four orthoimages. Illumination differences are evident between image sequences 1-2, and 3-4, which were photographed approximately two years apart [19].

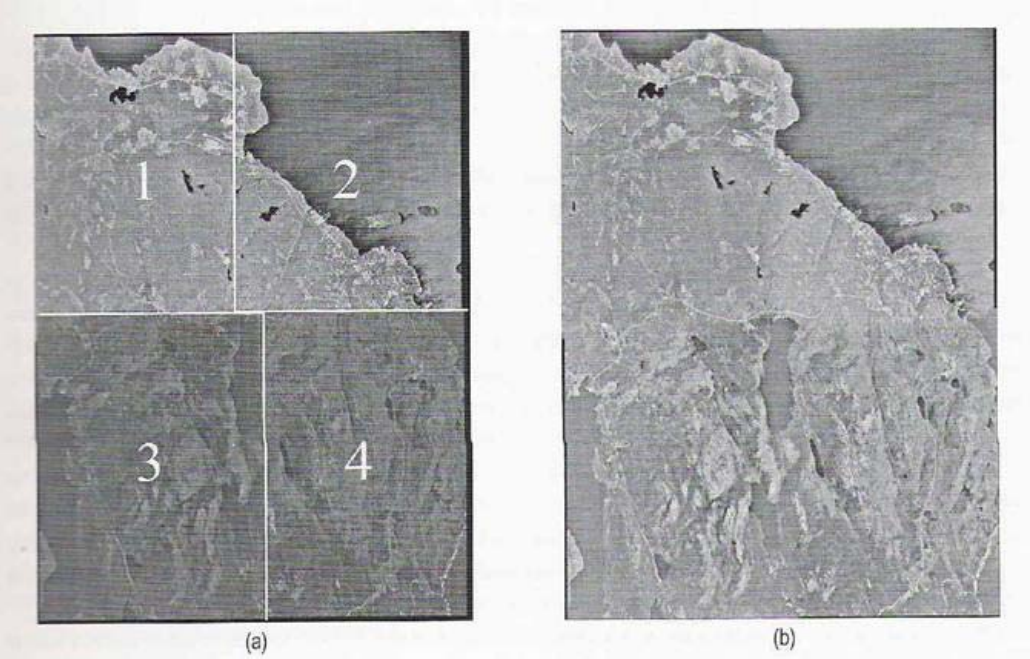

Figure 3.6: Histogram matching**.** (a) Input orthoimages: (1-2) photographed July 1994, and (3-4) photographed May 1996, (b) Mosaic performed with histogram matching [19].

3.4. True Orthophoto

The generation of True-Orthophotos has to consider the orthogonal projection with a DSM, the detection of occluded areas and the filling up of the occluded areas by taking the missing image parts from overlapping orthophotos. Assuming an error free georeference of the source image, e.g. aerial image, the ortho-projection basically is as accurate as its underlying surface model. And this phrase contains already the main topic, i.e. "surface model". In case of having a DSM available the man-made objects will be projected to the geometrically correct position. Fig. 3.7 shows the scheme of the orthoprojection with a DSM, which is a perpendicular parallel projection.

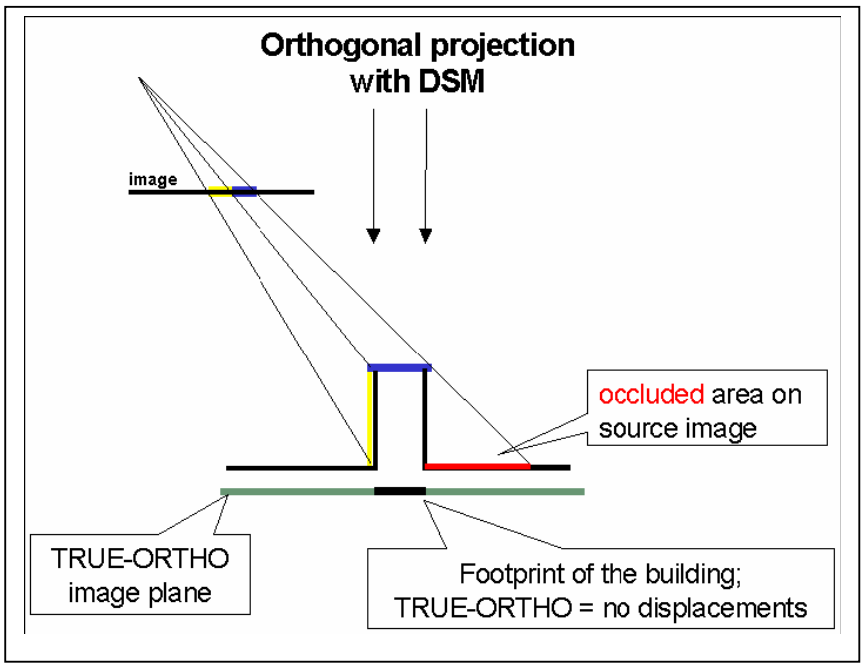

Figure 3.7: Scheme of true orthophoto projection with a DSM [20]

The problem is that areas occluded by the manmade objects are not visible in the image. In fig. 3.8.a the roof of the building also covers the occlusion area in the aerial source image. If such areas are not detected by the orthophoto rectification software the ortho-projection will just fill it up with image content from the same image. This then leads to so-called ghosting effects [20]. The orthophoto in fig. 3.8.b shows such ghosting effects.

Ghost images: The roofs of buildings are superimposed onto the bottom of the buildings and the roofs of buildings appear twice. This phenomenon is called “ghost image”. The reason causing ghost images is due to the fact that when we orthorectify the relief displacement caused by buildings, the roofs of buildings are orthorectified in their upright positions; when we orthorectify the relief displacement caused by occluded objects, the occluding objects are again employed to fill the occluded objects. This kind of processing process leads to the occluding pixels to be doubly employed [21].

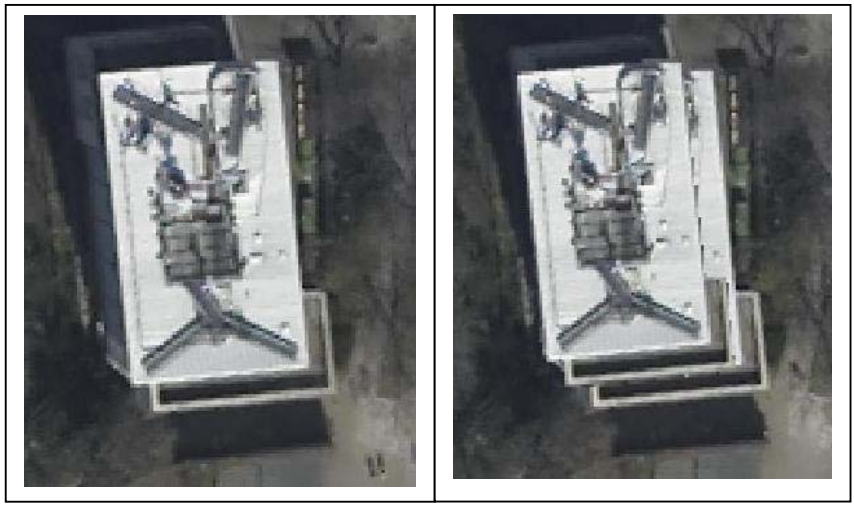

Figure 3.8: (left) Orthophoto and (right) Ghost effect

3.4.1 Detection and filling occluded areas

In order to fill occluded areas or, blind spots, imagery of these missing areas is needed. These supplemental images can be created by using images of the same area taken from different locations (fig. 3.9.a). This will result in different relief displacement in each image and by combining the images full coverage can be obtained. In aerial photography it is normal to let them images overlap as illustrated on fig. 3.9.b.

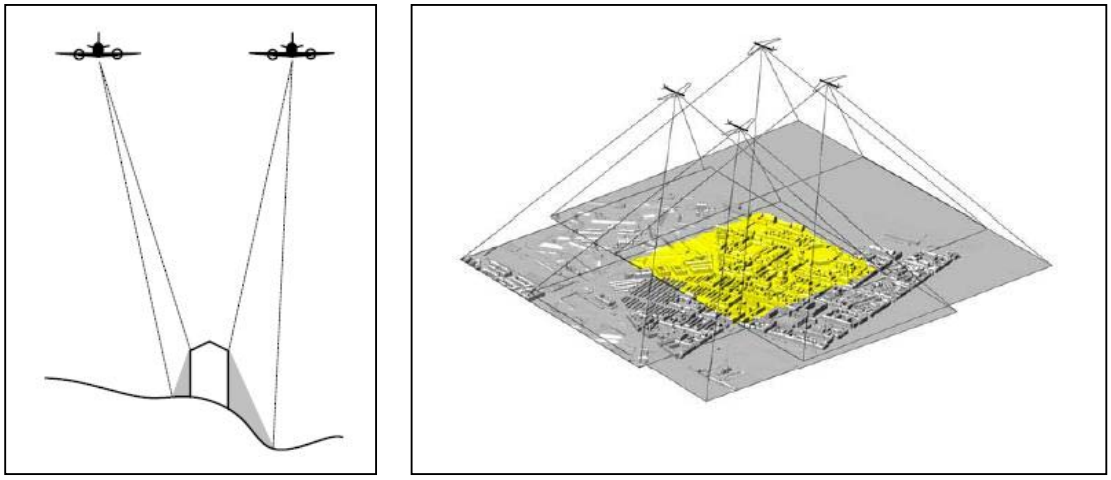

Figure 3.9: (a) (left) Combining several images to full coverage and (b) Aerial photography with %60 forward and side overlap. The four images above, all cover the same yellow area, but viewed from different locations. Buildings in the yellow

area will all have relied displacement in different directions so that blind spots hidden in one image is most likely visible in another [18].

4. PROPOSED ALGORITHM

4.1. Automatic Approach for the True Orthophoto Production:

As mentioned previous chapter, even though the orthophoto imagery eliminates the relief displacement effects on the terrain, man made objects like a building still leaning away from the image centre (nadir point) due to the terrain does not include the buildings or any other objects above the ground. True orthophoto imagery is produced to overcome these deficiencies.

In this approach, the advantage of LIDAR data, including dense reliable 3D information of buildings, was taken to create efficient DSM for the true orthophoto production purposes. On the other hand, both first pulse and last pulse of LIDAR measurements contain sufficient 3D information for the DSM generation (see also fig. 4.1.a and 4.1.b), the difference between them is known as the presence of trees. Commonly, last pulse is preferred to generate DTM or DSM due to most likely reflecting over the terrain surface beneath [7]. In this study, true orthophoto was produced by using first pulse surface model and last pulse surface model separately for the comparison purposes.

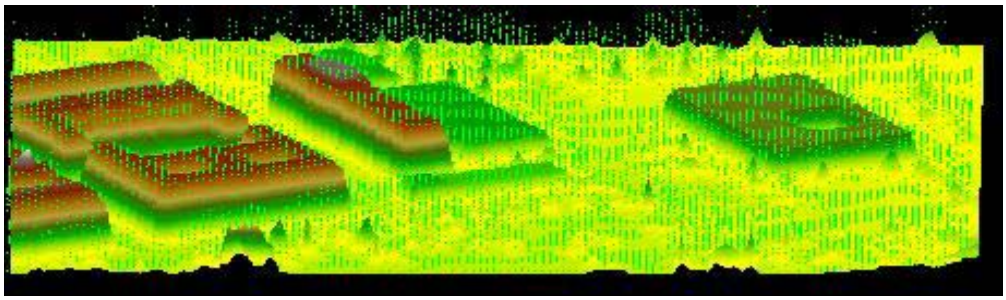

Figure 4.1: (a) DSM from first pulse measurement

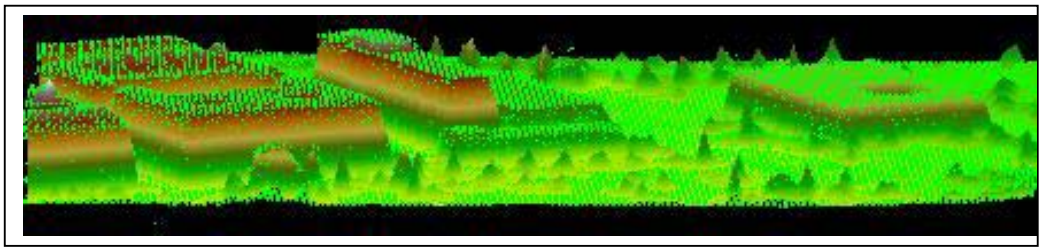

Figure 4.1: (b) DSM from last pulse measurement

For the true orthophoto production, the first task is to run rectification process based on reprojection by taking the DSM with (RGB) digital aerial images into account. For this purpose, provided project file which includes orientation parameters of digital aerial images was defined with image blocks into the photogrammetric system (see fig. 4.2.a). Additionally, the digital aerial images and corresponding orientation parameters may be checked and edited in the event of any inconsistency by the some extension tools of software (see fig. 4.2.b). Afterwards, DSM was created within 1 meter (m) dense from the laser grid points and imported into the project for the needs of true orthophoto production (see also fig. 4.2.c). Ground resolution of DSM has to be determined by considering the application area. In the case of urban areas, if the covered area of the roofs or dormers is smaller than the ground resolution of modelled DSM, some of the dormers or nested roofs might be ignored during the rectification process. Therefore, DSM was modelled in 1m dense for the production of true orthophoto in this study.

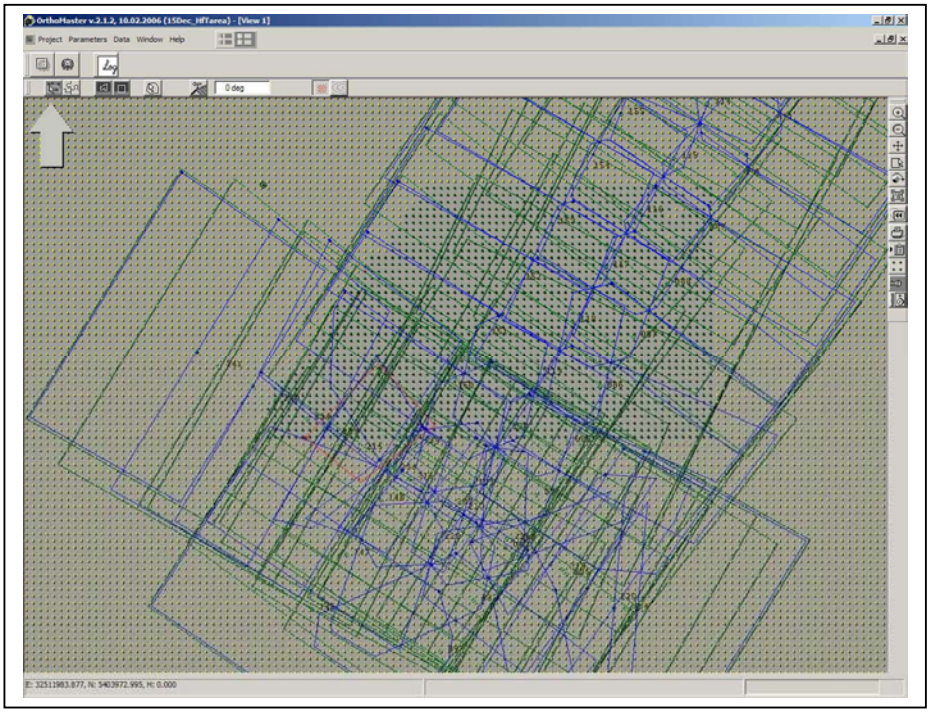

Fig. **Figure 4.2:** (a) Rectification Process by OrthoMaster System

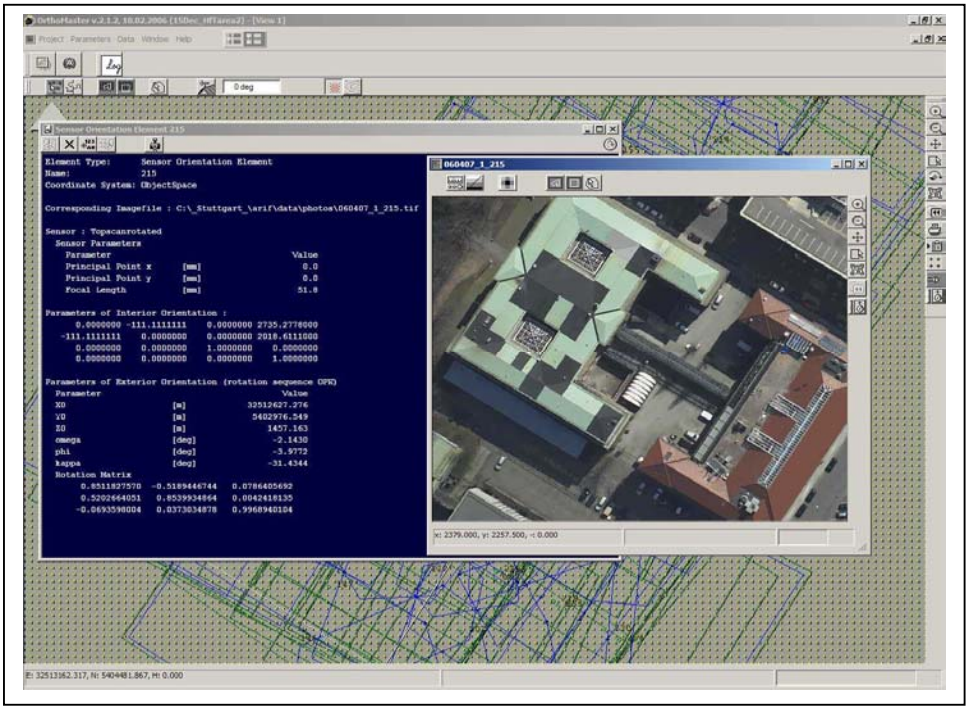

Fig. 4.2: (b) Image models and orientation parameters

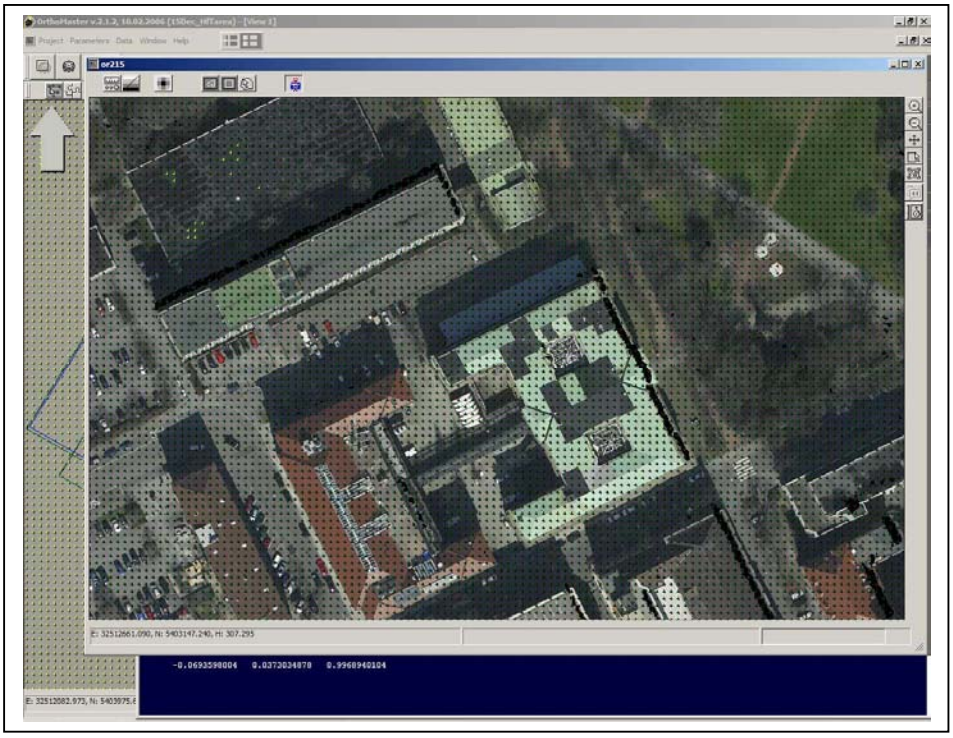

Figure 4.2: (c) The integration of DSM with Digital Aerial Images for the Rectification Process

Rectification process was done by two steps. In the first step, pixels from the input images were projected onto the corresponding position on the ground surface (DSM) based on collinearity equation. Then, the matched pixel were reprojected onto the map plane (true orthophoto) based on orthogonal projection from the DSM (see also fig. 3.7 in chapter 3.4). In the second step, grey levels from the input pixels were interpolated and assigned to the output pixels by using a resampling method. Well-known resampling methods are nearest-neighbour, bilinear, and cubic convolution. In this research, bilinear method was used. Because, this method leads to less jagged edges and the overall look is smoother than the nearest neighbour option. As for cubic convolution method, resampling by cubic convolution appears visually similar to resampling by bilinear interpolation, but it requires the most computational times out of three methods (see fig. 4.3).

Figure 4.3: (a). The result of nearest-neighbour method

Figure 4.3: (b). The result of bilinear method

Figure 4.3: (c). The result of cubic convolution method

After the rectification process, although the man made objects were correctly placed, rectification process caused other shortcoming so-called occluded areas. As the buildings were rectified into the true locations, the occluded areas occurred on where the buildings were leaning before. Therefore, during the rectification process, the visibility map was checked to locate occluded areas. The rectification processes and visibility test ran simultaneously so that all occluded areas were marked as background colour in the image (see fig 4.4). As a result of rectification processes, all buildings were repositioned correctly and occluded areas were located in the overlapped orthophoto imagery.

The second task is to run mosaic process to fill all occluded areas and merge the overlapped orthophotos as a form of mosaic so-called "*True Orthophoto Imagery"*. All the resulting overlapped orthophotos after the rectification processes were taken into account for the mosaic process (see also fig. 4.5.a). In the first step, all parts of the occluded areas were filled with real image information which was visible in one of the adjacent orthophotos based on the results of the visibility test. In the second step, all overlapped orthophotos were merged as a form of mosaic where the seamlines defined from the software. Seamline definition is done by software

automatically (see fig 4.5.b). On the other hand, seamlines may be defined manually by human operator, but it is time consuming process. Additionally, in the resulting mosaic sometimes distorted buildings might occur like the effect of bending over caused by seamline definition. These deficiencies might be corrected by editing seamlines and reprocessing the mosaic (see fig. 4.6).

Figure 4.4: The rectification and visibility processes result

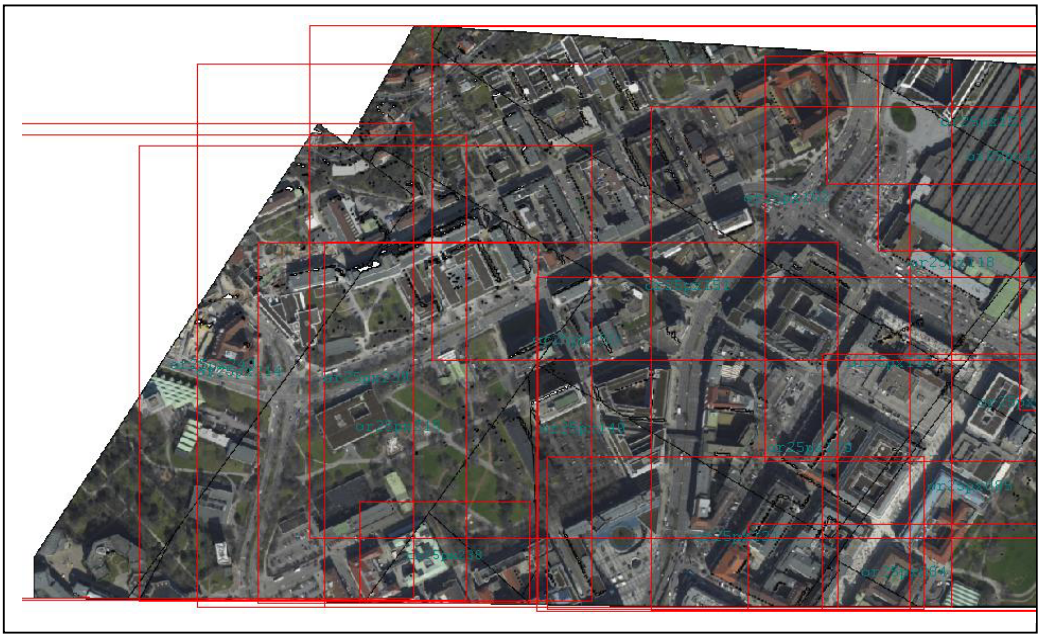

Figure 4.5: (a). Overlapped orthophotos are loaded, Mosaic Process by OrthoVista System

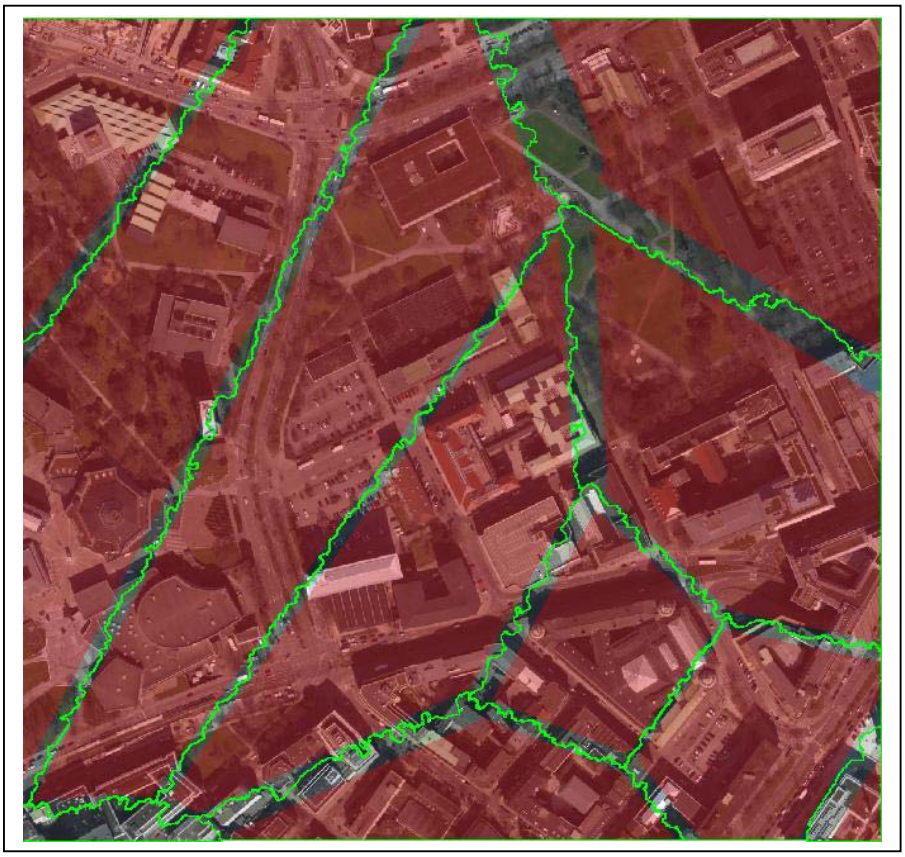

Figure 4.5: (b). Seamline definition for merging orthophotos

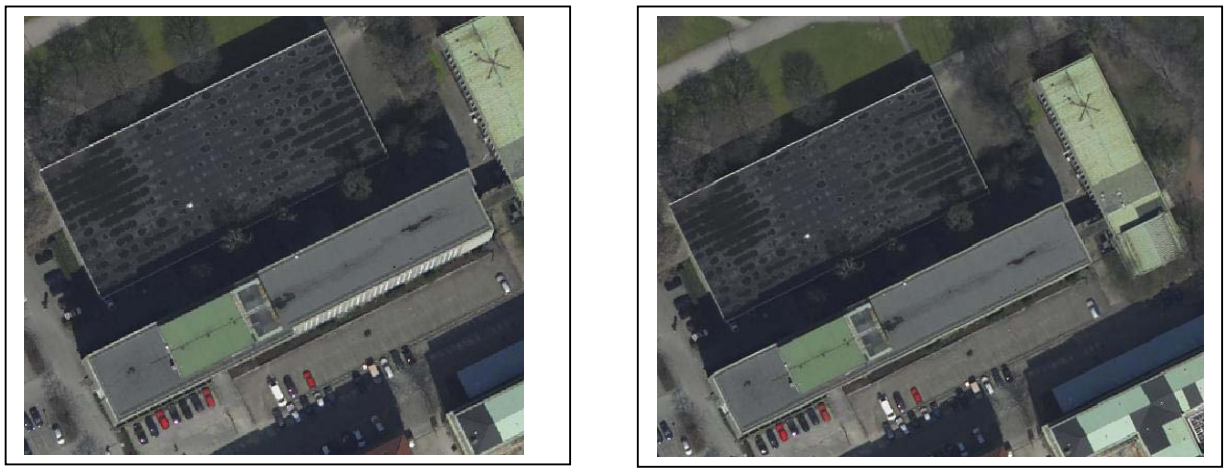

Figure 4.6: (right) previous mosaic, including distortion and (left) final mosaic after reprocessing

The main steps for the automatic true orthophoto production are summarized by the following workflow (Fig. 4.7):

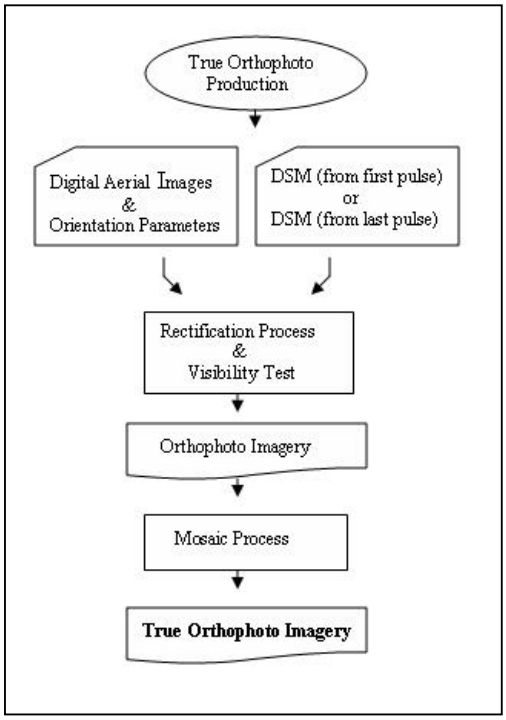

Figure 4.7: Workflow for the automatic true orthophoto production.

4.2. Semi Automatic Approach for the True Orthophoto Production

In the first approach, DSM was modelled only from the LIDAR data for the true orthophoto production purposes. Even though achievable true orthophoto overcame the deficiencies of orthophotos concerning the relief effects of buildings by using the DSM, roof borders and roof ridges of buildings were not represented in the realistic shape in the resulting true orthophoto. Almost all of the buildings suffered from the unsharp edges on the borders, especially on the ridges and edges of the roof. The experimental investigations with different data sets show that it is essential to use high quality DSMs to overcome such shortcomings.

In this semi automatic approach, for modelling of DSM not only utilized from LIDAR data but also digitized roof borders and ridges were used. Firstly, terrain texture was extracted from the LIDAR data instead of the surface texture so that 3D points of buildings and trees were removed (see fig. 4.8.a). Then, footprints of removed objects were filled in regular grid based on the specified dense parameter (in this case 1m dense) during the creation of DTM (see fig. 4.8.b). In the next step, roof borders and ridges were digitized in photogrammetric stereo workstation and superimposed on the DTM for the purpose of DSM creation (see fig. 4.8.c). Hence, DTM plus semi-automatically collected vector data were taken into account with the digital aerial images in order to generate true orthophoto in the second method (fig. 4.9.a).

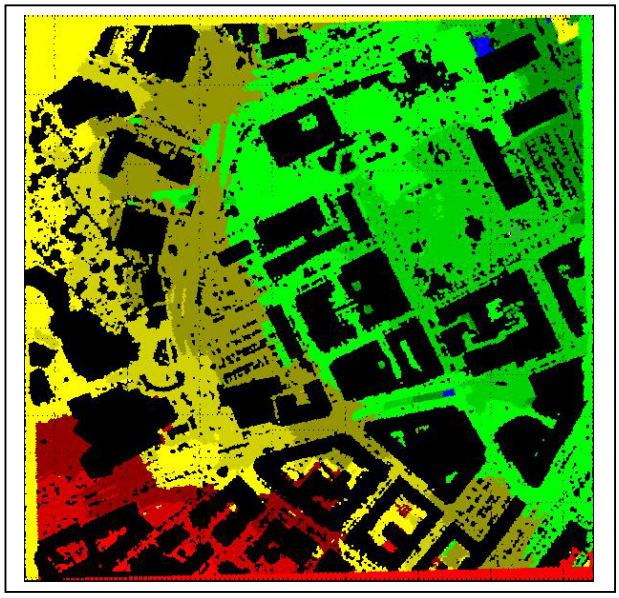

Figure 4.8: (a). Any objects above the ground are removed from the LIDAR data

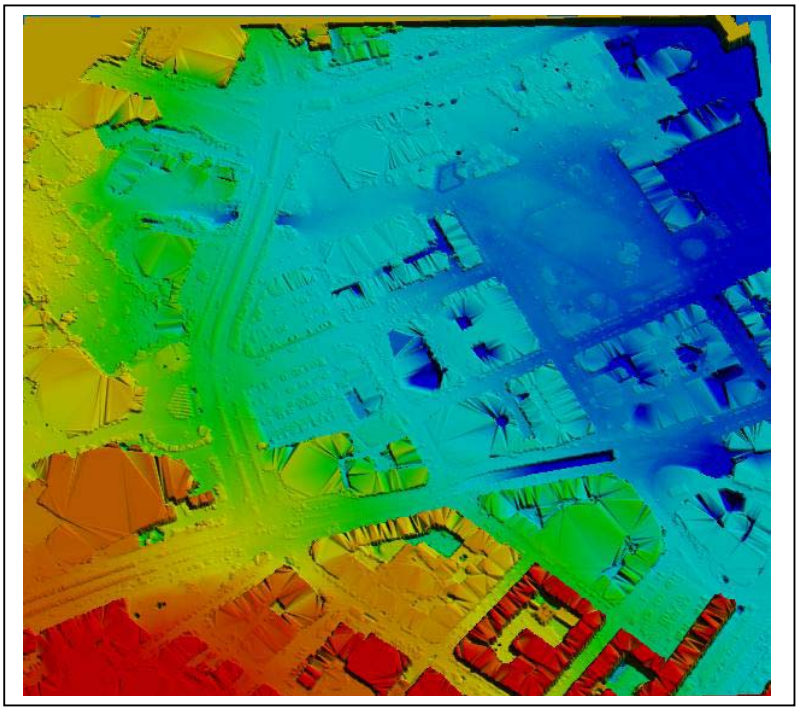

Figure 4.8: (b) DTM from laser points

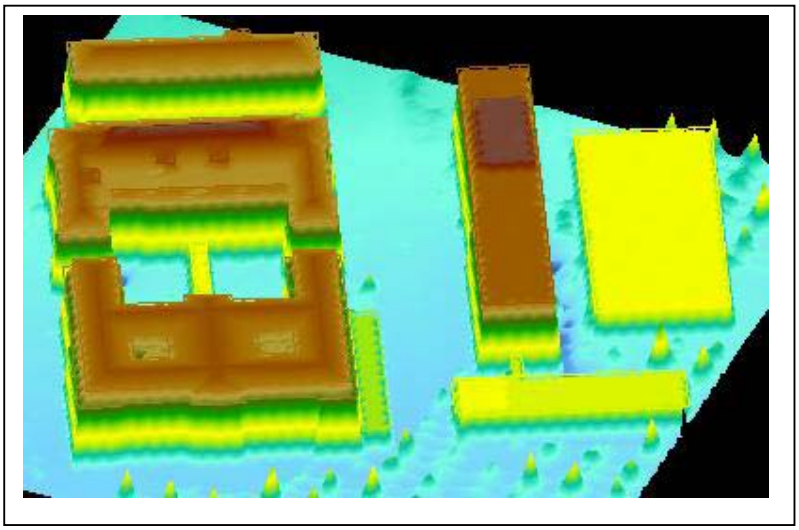

Figure 4.8: (c). DSM from the DTM plus border outlines

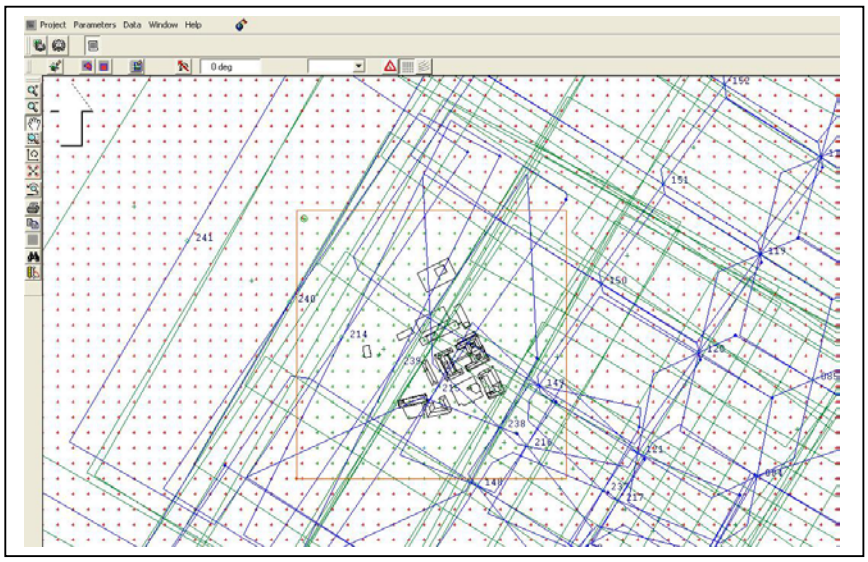

Figure 4.9: (a). Border outlines are imported for the rectification process

While the rectification process, building outlines of input images correctly matched with digitized building borders which had been blended in DTM so that man made structures were represented with realistic shape in true location in the resulting true orthophoto imagery (fig 4.9.b).

Figure 4.9: (b). Realistic representation of buildings by using border outlines

(0.25 cm pixel, 1m dense DSM)

Bilinear resampling method was used as in automatic approach so that an intensity value assigned to the output pixels by interpolating the gray levels from input pixels. Meanwhile, all occluded areas were marked and stored into visibility map after all rectification processes.

The last task of true orthophoto production is to merge all overlapped orthophotos and fill in occluded areas with real image information. Accordingly, mosaic process was run as mentioned first method so that all orthophotos were merged and occluded areas were filled.

The main steps for the semi automatic true orthophoto production are summarized by the following workflow (Fig. 4.10):

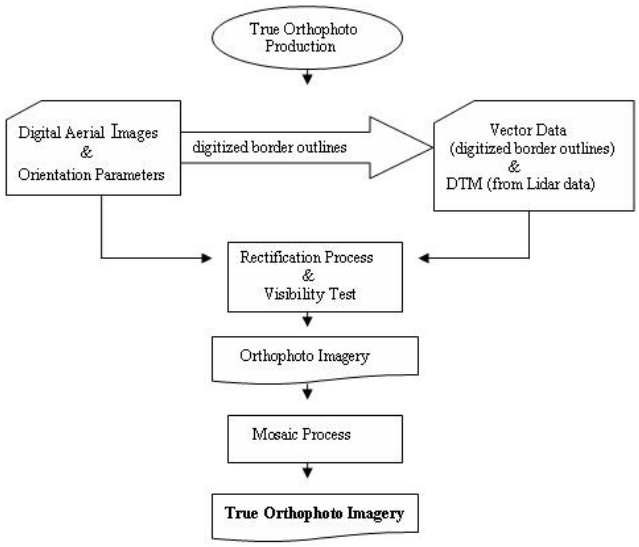

Figure 4.10: Workflow for the semi automatic true orthophoto production.

5. EXPERIMENTAL INVESTIGATIONS

For the experimental investigation a LIDAR test data and RGB digital images covers the downtown area of Stuttgart where is located the west of Germany were used. The test data sets have been provided by TopScan Company, in Germany. LIDAR test data has been recorded as the first pulse and the last pulse by ALTM 2050 Laser scanner with a density of 4.8 per m² on the average. RGB digital images have been taken simultaneously by using the Rollei AIC-modular-LS digital metric camera with a 20cm ground resolution.

The aim of the research was to eliminate the relief displacement effect of building in the traditional orthophoto caused by using DTM during the rectification processes. In the traditional orthophoto, man made structures like a building was incorrectly placed due to DTM does not including any man made structures (see fig 5.1.a). Accordingly, DSM was taken into account for the rectification process due to including digital building models as well as the terrain model. Thus, the relief displacement effect of buildings, especially for the tall buildings was eliminated in the traditional orthophoto (see fig. 5.1.d). However, the effect of double mapped objects occurred, so-called ghost effect caused by obscured areas. Because, during the rectification process, rays are reprojected back to both the occluded area and the obscuring object, without detecting that obscured data is being rectified. Therefore, if a building is repositioned correctly in a DSM, it will also leave a copy of a building on the occluded area in the terrain (see also fig 5.1.b). For this reason, during the rectification process visibility test was run simultaneously to locate occluded areas. Hereby, all occluded areas were marked by a specified colour (or default background colour) and ghost effect was removed in the resulting orthophoto (see fig 5.1.c). The last task was to fill all marked occluded areas with the corresponding real image information from the adjacent orthophotos. Therefore, mosaic process was run by taking all the overlapped orthophotos into account. Hence, all the occluded areas were filled whit the real image information from one of the adjacent orthophoto and merged them as a form of mosaic, so-called *"True Orthophoto Imagery"* (see also

fig. 5.1.d). After all processes, buildings were correctly placed into true locations and all occluded areas were filled with real image information in the resulting true orthophoto.

On the other hand, in the resulting true orthophoto also shows that borders of the building were not represented in realistic shape even the buildings were correctly repositioned. The edges of roofs were seen unsharp and blurred caused by quality of DSM (see fig 5.1.d).

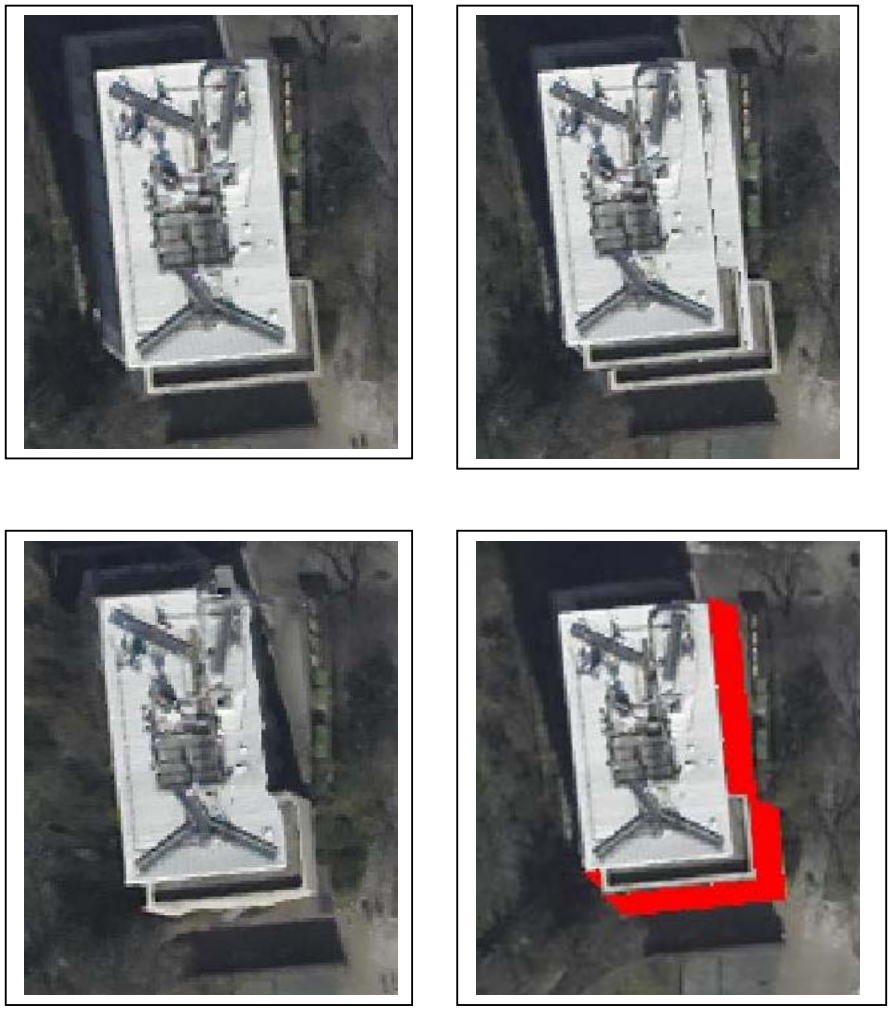

Figure 5.1: (a). Orthophoto (above-left) and (b). Ghost effect(above-right), (c). Visibility test result (below-right) and (d). True orthophoto (below-left). (0.25 cm pixel, 1m dense DSM)

For the aspect of automatic true orthophoto production, the DSM had been taken into account by using first pulse and last pulse measurement to observe the effects of

laser pulses on the quality of true orthophoto imagery. The achievable true orthophotos by using laser pulses separately showed that the relief displacement effect and occlusion problem were overcome easily. However, both resulting true orthophotos are suffer from the same fact that unsharp and blurred borders on the edge of the buildings and the roads (see fig. 5.2). On the other hand, fig. 5.2.a shows that borders of the man made structures, especially borders of the roads more blurred than the other true orthophoto which is shown fig. 5.2.b. These differences in the resulting true orthophotos are probably caused by differences in the presence of the 3D information in the first and last pulse measurement. These results showed that the best suit laser pulse is the last pulse measurement of LIDAR for the creation of DSM, then production of true orthophoto surely.

Figure 5.2: (a). True ortho photo from first pulse (0.25 cm pixel, 2m dense DSM)

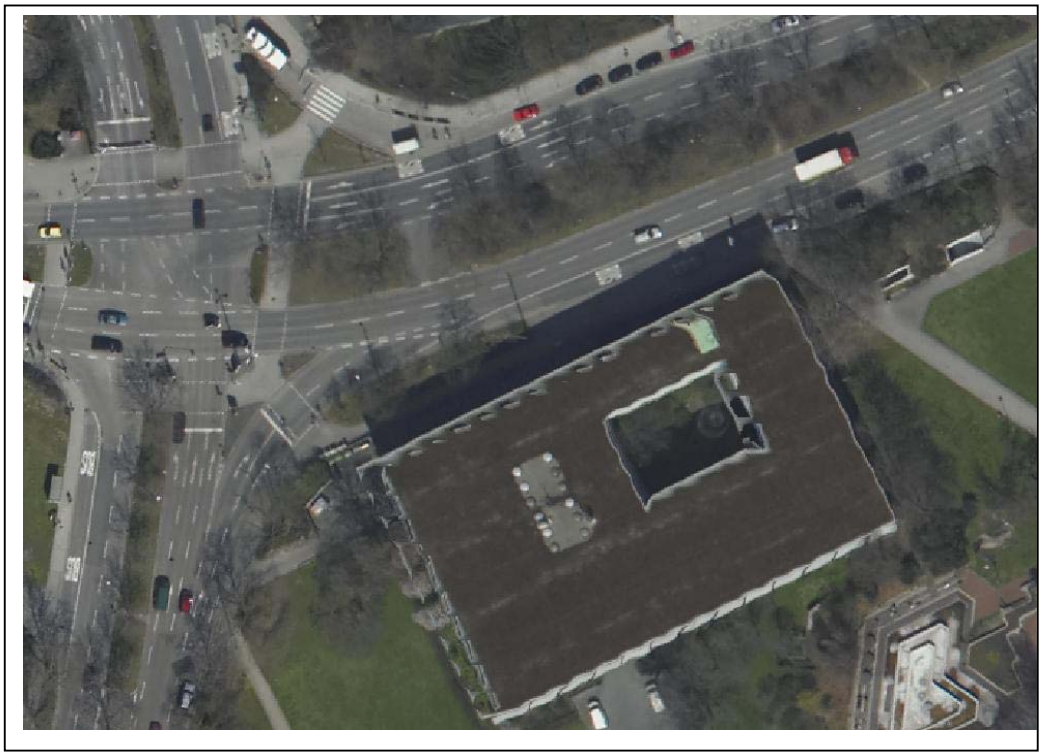

Figure 5.2: (b). True orthophoto from last pulse (0.25 cm pixel, 2m dense DSM)

As for the second approach results, the achievable true orthophoto showed that not only buildings were correctly placed into true locations but also the unsharp borders on the edge of buildings are overcome. Fig. 5.3.a shows that the previous true orthophoto based on the first approach and fig. 5.3.b shows that the resulting true orthophoto based on second approach so that two approaches may be observed comparatively. In fig. 5.3.b, it is clearly seen that roof edges and roof ridges were sharply represented in the resulting true orthophoto. As shown fig. 5.3.a, there are some distortions on the edges of the roofs, particularly on the nested roofs. Because, nested roof of buildings are made of glass so that the laser beams are not reflected properly from that part of building. This effect causes blunders or gaps in DSM so that in resulting true orthophoto these areas are seen as blurred and jagged edges (see fig. 5.3.a.). These deficiencies were overcome by blending digitized border outlines into the DTM instead of using DSM only from LIDAR. Thus, higher accuracy DSM was created for the true orthophoto production purposes. The achievable quality of true orthophoto represents the buildings in realistic shape (see fig. 5.3.b).

Figure 5.3: (a). First method (0.25 cm pixel, 1m dense DSM)

Figure 5.3: (b). Second method result (0.25 cm pixel, 1m dense DSM)

In the fig. 5.4, produced true orthophoto is draped over the DSM for the 3D visualization purposes of test area.

Figure 5.4: Visualization of a part of test area

6. CONCLUSIONS

Two methods, automatically and semi automatically true orthoohoto production were investigated in this comparative study. DSM was modeled in two different ways for the purpose of improving true orthophoto quality.

The automatic method is a fast and efficient method for the generation of true orthophoto based on DSM (only from LIDAR data). The achievable result gives an approximation about building features in correct position, but not realistic representation. This effect probably comes from some blunders and gaps in LIDAR data set. Because laser beams might be scattered or not reflected from the target like glass structures, so positions are sometimes obtained wrongly. This may causes such deficiencies in the resulting true orthophoto considering the large urban areas. On the other hand, DTM plus delineated borders of buildings were used as DSM to make use of accurate digital building models for the true orthophoto production in the semi automatic method. In this resulting true orthophoto, realistic representations of buildings were achieved by using mixed data for the creation of DSM.

As a result, this experimental investigation shows that derived DSM only from LIDAR data is sometimes not sufficient for the production of true orthophoto imagery in the urban areas.

Accuracy of true orthophoto is strongly dependent to accuracy of DSM. Therefore, DSM should be modelled by blending the building outlines with DTM (from LIDAR data), for the production of high quality true orthophoto purposes.

REFERENCES

[1] **You, S., Hu, J., Neumann U. and Fox, P.,** 2003. Urban site modeling from LIDAR, *Springer-Verlag Berlin Lecture Notes In Computer Science*, Vol. 2669, pp. 579-588.

[2] **Haala, N., Brenner, C. and Anders, K.,** 1998. 3D urban GIS from laser altimeter and 2D map data, *ISPRS Commission III Symposium on Object Recognition and Scene Classification from Multispectral and Multisensor Pixels,* Columbus, Ohio, pp. 339-346.

[3] **Kim, Changjae., Ghanma, Mwafag. and Habib, A.,** 2006. Integration of Photogrammetric and LIDAR data for realistic 3D model generation, *First International Workshop On Mobile Geospatial Augmented Reality,* Alberta, Canada, May 29-30.

[4] **Albertz, J. and Wolf, B.,** 2006. Generating true orthoimages from urban areas without height information, *1st EARSeL Workshop of the SIG Urban Remote Sensing,* Berlin, Germany, March 2-3.

[5] **Deng, F., Zhang, Z. and Zhang, J.,** 2005. Construct 3D model by multi-sensor data, *ISPRS work shop on Service and Application of Spatial Data Infrastructure,* Vol. XXXVI (4/W6), Hangzhou, Chine, October 14-16.

[6] **TopScan GmbH**, www.topscan.de visited on April 2007.

[7] **Inpho GmbH**, www.inpho.de visited on April 2007.

[8] **Sangster C.,** 2001. Validating LIDAR - Evaluating LIDAR accuracy using GPS, *Applied Geomatics Research Group Centre of Geographic Sciences Lawrencetown,* Nova Scotia.

[9] **URL:** http://www.fergi-online.de/angebot/module/index.html visited on April 2007.

[10] **Sapeta, K.,** Have you seen the light?, [Online], http://www.sanborn.com/Pdfs/Article_Have_You_Seen_Medres.pdf.

[11] **C, Crosby.,** 2006. A geoinformatics approach to LIDAR data distrubition and processing for the earth sciences, *Fall '06 SESE Geomorphology seminar*.

[12] **Harding, J.D.,** 2000. Principles of airborne laser altimeter terrain mapping, *NASA's Goddard Space Flight Center,* March 17.

[13] **Arefi, H., Hahn, M. and Lindenberger, J.,** 2003. LIDAR data classification with remote sensing tools, *Commision IV Joint Workshop on Challenges in Geospatial Analysis, Integration and Visualization II*.

[14] **Sithole, G.,** 2005. Segmentation and classification of airborne laser scanner data, Ph.D. Thesis, *Publications on Geodesy 59 NCG Nederlandse Commissie voor Geodesie Netherlands Geodetic Commission Delft*.

[15] **Schickler, W. and Thorpe, A.,** 2001. Surface estimation based on LIDAR, *Proceedings of the ASPRS Annual Conference. St. Louis,* Missouri, April 2001.

[16] **Arens, C.,** Airborne laser scanning, M.Sc. Thesis, *Geodynamics Department of The National Survey and Cadastre*, Copenhagen, May 24, 2002.

[17] **Thorpe, A.,** 2001. Digital orthophotography in new york city, [Online], http://www.sanborn.com/Pdfs/Article_DOI_Thorpe.pdf.

[18] **Nielsen, O.M.,** True orthophoto generation, 2004. *Informatics and Mathematical Modelling in Technical University of Denmark.*

[19] **American Society of Photogrammetry,** 2004. Manual of Photogrammetry, Fifth Edition, *American Society of Photogrammetry*, Bethesda, Maryland.

[20] **Braun, J.,** Aspects on true orthophoto production, 2003. *INPHO GmbH*, *Photogrammetric Week 2003*, Stuttgart, Germany.

[21] **Zhou, G. and Chen., W.,** Urban image true orthorectification in the national map program*, Tempe, AZ,* USA, March 14-16 2005.

CURRICULUM VITAE

Was born in 1982 in Antalya. He has graduated from Antalya Karatay High School. In 2000 he has begun to study in Geodesy and Photogrammetry Engineering Department of the Civil Engineering Faculty at ITU. He has graduated in 2005 and has begun his master degree in Institute of Science and Technology at ITU. He has been at Stuttgart University Applied Sciences for his thesis research in 2007.